Geological Society of America Bulletin

Constraining landscape history and glacial erosivity using paired cosmogenic nuclides in Upernavik, northwest Greenland

Lee B. Corbett, Paul R. Bierman, Joseph A. Graly, Thomas A. Neumann and Dylan H. Rood

Geological Society of America Bulletin published online 23 July 2013;
doi: 10.1130/B30813.1

Notes

Geological Society of America Bulletin, published online on 23 July 2013 as doi:10.1130/B30813.1

Constraining landscape history and glacial erosivity using paired cosmogenic nuclides in Upernavik, northwest Greenland

Lee B. Corbett[1,†], Paul R. Bierman[1], Joseph A. Graly[1,§], Thomas A. Neumann[1,#], and Dylan H. Rood[2,3]
[1]*Department of Geology, University of Vermont, Burlington, Vermont 05405, USA*
[2]*Scottish Universities Environmental Research Centre (SUERC), East Kilbride G75 0QF, UK*
[3]*Earth Research Institute, University of California, Santa Barbara, California 93106, USA*

ABSTRACT

High-latitude landscape evolution processes have the potential to preserve old, relict surfaces through burial by cold-based, nonerosive glacial ice. To investigate landscape history and age in the high Arctic, we analyzed in situ cosmogenic ^{10}Be and ^{26}Al in 33 rocks from Upernavik, northwest Greenland. We sampled adjacent bedrock-boulder pairs along a 100 km transect at elevations up to 1000 m above sea level. Bedrock samples gave significantly older apparent exposure ages than corresponding boulder samples, and minimum limiting ages increased with elevation. Two-isotope calculations (^{26}Al/^{10}Be) on 20 of the 33 samples yielded minimum limiting exposure durations up to 112 k.y., minimum limiting burial durations up to 900 k.y., and minimum limiting total histories up to 990 k.y. The prevalence of ^{10}Be and ^{26}Al inherited from previous periods of exposure, especially in bedrock samples at high elevation, indicates that these areas record long and complex surface exposure histories, including significant periods of burial with little subglacial erosion. The long total histories suggest that these high-elevation surfaces were largely preserved beneath cold-based, nonerosive ice or snowfields for at least the latter half of the Quaternary. Because of high concentrations of inherited nuclides, only the six youngest boulder samples appear to record the timing of ice retreat. These six samples suggest deglaciation of the Upernavik coast at 11.3 ± 0.5 ka (average ± 1 standard deviation). There is no difference in deglaciation age along the 100 km sample transect, indicating that the ice-marginal position retreated rapidly at rates of ~120 m yr^{-1}.

INTRODUCTION

The surface morphology of many high-latitude landscapes is a product of not one, but numerous glacial-interglacial cycles (Sugden, 1977, 1978; Sugden and Watts, 1977). Because areas in Greenland, the Canadian Arctic, and Scandinavia are periodically covered by cold-based glacial ice and snowfields, bedrock surfaces evolve over hundreds of thousands of years and through repeated burial by nonerosive glacial ice (Anderson et al., 2000; Bierman et al., 1999; Blake, 1970; Briner et al., 2003, 2006; Harbor et al., 2006; Kleman, 1992; Kleman and Borgstrom, 1994; Marquette et al., 2004; Stroeven et al., 2002a, 2002b; Sugden et al., 2005). This implies that high-latitude landscapes may preserve relict surfaces that formed hundreds of thousands or even millions of years ago.

Study of these old glacial landscapes is important for understanding the time scales and processes of high-latitude landscape development; however, such studies are challenging because the complex exposure and burial histories of rock surfaces in these areas violate the assumptions of many chronological techniques such as traditional ^{10}Be surface exposure dating. Here, we employ analysis of paired cosmogenic nuclides (^{10}Be and ^{26}Al) in adjacent bedrock and boulder samples to study the age and history of the landscape in Upernavik, northwest Greenland. We aim to understand the age of rock surfaces, durations of exposure and burial, efficiency of subglacial erosion, and rate of latest Pleistocene ice-margin retreat in a landscape characterized by deep fjords and extensive uplands.

Glaciers can erode their beds in a number of different ways, including abrasion and plucking. However, most forms of subglacial erosion require basal ice to be at its melting point; this enables processes such as basal sliding, regelation, and freeze-on of rock and sediment to operate (Herman et al., 2011). Warm-based glaciers, for which the basal temperature is at the pressure melting point, can erode their beds, but under cold-based glaciers, where the basal temperature does not reach the pressure melting point, little erosion occurs (Sugden, 1978). Although exceptions have been noted (Atkins et al., 2002; Cuffey et al., 2000; Waller et al., 2012), it is generally accepted that episodes of burial caused by cold-based glacial ice are incapable of removing sufficient material to expose fresh rock surfaces after glaciation.

Measurement of in situ–produced cosmogenic nuclides can provide information about landscape history and chronology (Balco, 2011; Fabel and Harbor, 1999). Production of ^{10}Be and ^{26}Al is dominated by nuclear spallation, which occurs when high-energy particles impact the nuclei of ^{16}O and ^{28}Si atoms in quartz, respectively. This impact causes material to be ejected from the nucleus, leaving behind the lighter isotopes, ^{10}Be and ^{26}Al. Spallation-induced cosmogenic nuclide production in rock surfaces decreases exponentially with depth, with the rate of decrease depending on the density of the material. The attenuation length of high-energy neutrons is ~160 g cm^{-2}; thus, the highest concentrations of cosmogenic nuclides are produced in the upper several meters of rock. Efficient glacial erosion removes this preexisting inventory by abrading or plucking the rock's surface.

In areas where glacial ice has not completely eroded the preexisting exposure history, analysis of paired ^{10}Be and ^{26}Al data can be used to

[†]Present address: Department of Earth Sciences, Dartmouth College, Hanover, New Hampshire 03755, USA; e-mail: Ashley.Corbett.GR@dartmouth.edu.
[§]Present address: Department of Geology and Geophysics, University of Wyoming, Laramie, Wyoming 82071, USA.
[#]Present address: National Aeronautics and Space Administration Goddard Space Flight Center, Cryospheric Sciences Branch, Greenbelt, Maryland 20770, USA.

 doi:10.1130/B30813.1; 14 figures; 2 tables; Data Repository item 2013264.

make inferences about landscape age, exposure and burial durations, and subglacial erosion efficiency (Bierman et al., 1999; Briner et al., 2003;, 2006; Briner and Swanson, 1998; Goehring et al., 2010; Harbor et al., 2006; Marquette et al., 2004; Nishiizumi et al., 1991; Roberts et al., 2009; Stone and Ballantyne, 2006; Stroeven et al., 2002b; Sugden et al., 2005). If a landscape also contains areas where glacial ice has stripped at least ~2–3 m of material from rock surfaces (Balco, 2011), sufficient to remove most nuclides from previous periods of exposure, ^{10}Be surface exposure dating of glacially transported boulders and abraded bedrock can give estimates of the timing and rate of ice-margin retreat (Briner et al., 2009; Gosse et al., 1995a; Hughes et al., 2012; Kelly et al., 2008; Nishiizumi et al., 1991; Phillips et al., 1990; Young et al., 2011).

To understand the history of the landscape near Upernavik, northwest Greenland, we used an experimental design incorporating paired bedrock and boulder samples, paired ^{10}Be and ^{26}Al analyses, and samples collected at different elevations and different distances from the ice-sheet margin. This approach allowed us to make inferences about both subglacial erosion efficiency and the timing of ice-margin retreat during the latest Pleistocene deglaciation.

STUDY SITE AND PREVIOUS WORK

The Upernavik region (~73°N, 55°W; Fig. 1) is characterized by dissected terrain that encompasses table-top–shaped islands up to 1 km above sea level separated by deep fjords, including the large Upernaviks Isfjord to the north. Fjord depths are not well constrained; however, water depth in Upernaviks Isfjord is thought to be ~700 m (Peterson, 2003). The present-day ice margin lies ~100 km to the southeast of the outermost islands. The bedrock in the Upernavik area is predominately granite and granite pegmatite, some of which is weakly foliated; younger basalt flows cover the granite toward the southeastern end of the field area (Escher and Pulvertaft, 1995).

A pronounced contrast exists between the low-elevation and high-elevation landscapes. Much of the low-elevation bedrock is glacially streamlined (Fig. 2), although striations and glacial polish were not observed at the locations we visited. Conversely, many of the high-elevation bedrock forms exhibit pronounced surface weathering features (Fig. 3), including pedestals up to 10 cm in height, weathering pits, and pervasive frost shattering. At high elevations, much of the bedrock erodes by breaking into sheets that range from several centimeters to several tens of centimeters thick, and in many cases surfaces are mantled with grus. Both low- and high-elevation surfaces are covered with perched boulders.

Previous dating constraints on deglaciation of the Upernavik region are based on radiocarbon measurements in detrital organic material (Fig. 1); however, data from this region are relatively sparse in relation to the rest of Greenland's coast (Bennike and Björck, 2002). A basal radiocarbon age from a lake on Svartenhuk Halvø, the large peninsula of land ~1° south of Upernavik, provides a minimum deglaciation age of 10.4–10.2 cal ka B.P. (Bennike, 2000). Farther away in Melville Bugt, ~2° north of Upernavik, a whale vertebra found on recently deglaciated terrain yielded a radiocarbon age of ca. 9.3–9.0 cal ka B.P. (Bennike, 2008). The vertebra was likely deposited on the ocean floor after the whale's death and incorporated into the ice sheet during a later readvance. Bennike (2008) infers that, by ca. 9.3–9.0 ka, the ice-sheet margin at Melville Bugt was similar to or behind its present-day position, indicating that the coast had been deglaciated by the early Holocene. Also near Melville Bugt, a basal radiocarbon age from a lake sediment core yielded a minimum deglaciation age of ca. 9.9–9.3 cal ka B.P. (Bennike, 2008; Fredskild, 1985), and a radiocarbon age from shell fragments in marine sediment gave an age of ca. 9.0–8.5 cal ka B.P. (Bennike, 2008; Kelly, 1980).

USING COSMOGENIC NUCLIDES TO UNDERSTAND GLACIAL EXPOSURE AND EROSION

Theoretical Background

Measurement of in situ–produced cosmogenic nuclides is a useful technique for understanding the timing of surface exposure and burial, as well as the efficiency of subglacial erosion. Because cosmogenic radionuclides, such as ^{10}Be and ^{26}Al, form at known rates in

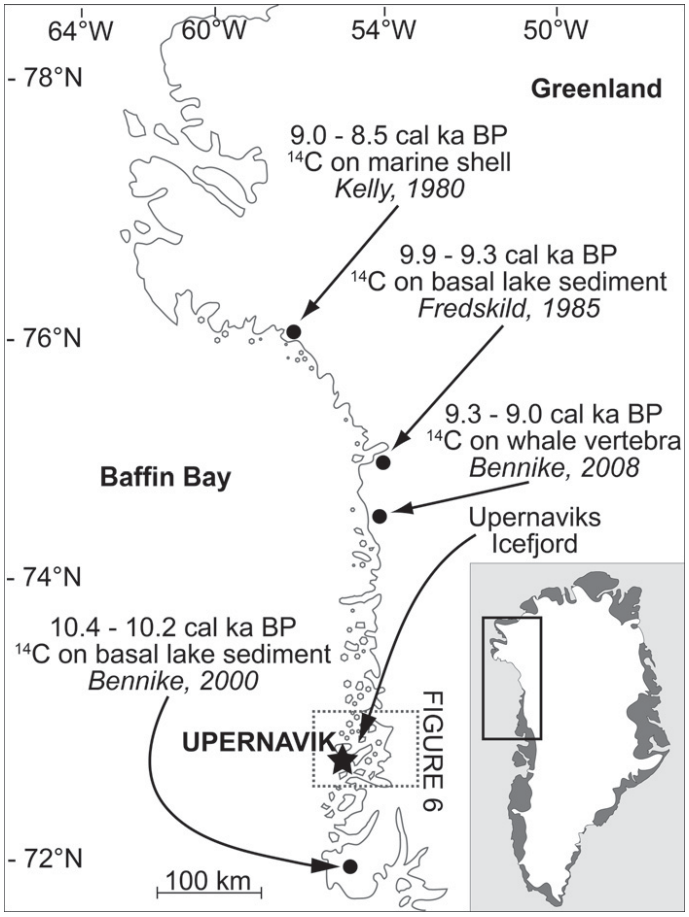

Figure 1. Regional map of central-western and northwestern Greenland. The small box shows the location of the study site as shown in Figure 6. Black dots indicate radiocarbon ages as described in the text.

Figure 2. Low-elevation locations are characterized by streamlined bedrock forms and abundant perched boulders. No glacial striations or polish were observed. Photograph by P. Bierman.

minerals bombarded by cosmic rays (Lal, 1988), quantifying the nuclide concentration in a sample allows inferences to be made about that sample's exposure history (Balco, 2011; Gosse and Phillips, 2001). In the simplest case, a surface is rapidly exposed to cosmic radiation after being buried beneath material sufficiently thick to block most cosmogenic nuclide production (e.g., many meters of glacial ice). The concentration of cosmogenic nuclides can then be used to determine when exposure occurred if the surface has not been eroded (Balco, 2011).

Figure 3. High-elevation locations exhibit evident surface weathering features including pedestals, weathering pits, frost shattering, abundant grus, and sheet weathering. Photograph by P. Bierman.

Analysis of two cosmogenic isotopes with different half-lives can provide information about complex exposure and burial histories (Granger and Muzikar, 2001; Nishiizumi et al., 1989, 1991). In the case of the two isotopes employed here, ^{26}Al is produced ~6.75 times as rapidly as ^{10}Be, although the uncertainty of the production ratio is not well constrained, and recent work has suggested that the ratio may actually be closer to ~6.9–7.0 (Argento et al., 2013). Once a sample is buried and nuclide production ceases, the ^{26}Al/^{10}Be ratio will drop from 6.75 because the half-life of ^{26}Al (0.71 m.y.) is less than that of ^{10}Be (1.36 m.y.). If a sample is exposed again following burial, production resumes, and the ^{26}Al/^{10}Be ratio increases.

The ^{26}Al/^{10}Be ratio data are commonly shown on a two-isotope plot, in which the vertical axis is the isotope ratio and the horizontal axis is the concentration of one of the measured isotopes, usually ^{10}Be (Fig. 4). On this diagram, samples that have been continuously exposed plot along a "constant exposure" line characterized by slowly decreasing ^{26}Al/^{10}Be ratio but increasing ^{10}Be inventory (Fig. 4). When a sample is buried, its position on the diagram travels leftward and downward from the constant exposure line, along a path characterized by both decreasing ^{26}Al/^{10}Be ratio and ^{10}Be inventory (Fig. 4). Although any inverse solution is nonunique (the measured isotope concentrations could result from an infinite number of different exposure-burial scenarios), two-isotope data can be used to calculate the most parsimonious solution: a minimum duration of initial exposure followed by a minimum duration of burial (Bierman et al., 1999; Briner et al., 2006; Håkansson et al., 2008; Lilly et al., 2010; Stroeven et al., 2002b; Sugden et al., 2005).

If samples have been re-exposed following burial (for example, during the Holocene period), the assumption of a single period of exposure followed by a single period of burial is violated. In these cases, minimum limiting exposure durations, burial durations, and total histories can be corrected for Holocene exposure by excluding the most recent period of nuclide production from the calculations. The minimum age of perched boulders free of inherited nuclides can provide an estimate of the timing of deglaciation and can be used to determine the duration of Holocene exposure for which this correction should be applied.

Application of the Two-Isotope Approach to Glacial Landscapes

The two-isotope approach has proven to be useful for investigating landscapes where surfaces at high elevation appear to be significantly

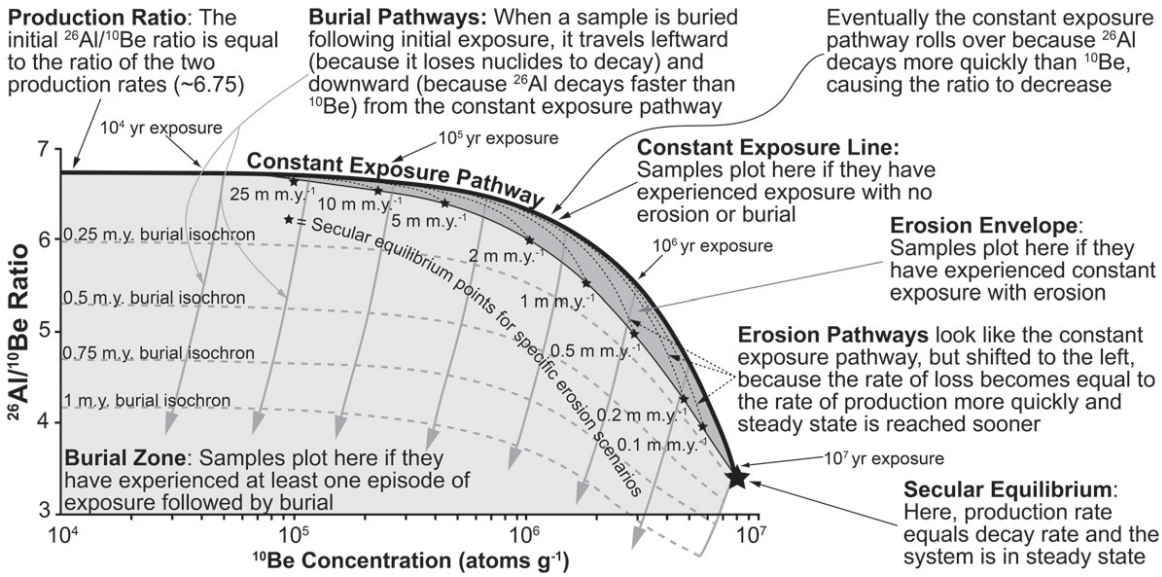

Figure 4. Schematic depiction of how two-isotope cosmogenic data are plotted, with explanations about important processes and the ways in which they are manifested in the isotope data.

more weathered than surfaces at low elevation (Dyke, 1979; Sugden, 1977, 1978). In particular, this technique can be employed to distinguish between two different scenarios: continuous exposure of uplands to subaerial weathering versus long-term preservation of uplands beneath intermittent cover by nonerosive glacial ice.

If the ice is not thick enough to cover the landscape completely, the highest upland surfaces are continuously exposed as nunataks (Dyke, 1979). In this case, high-elevation samples have old single-nuclide minimum limiting exposure ages, close agreement between bedrock and boulder samples, and $^{26}Al/^{10}Be$ ratios that are indistinguishable from constant exposure. This scenario has been documented in southwestern Greenland (Roberts et al., 2009); such high-elevation surfaces protruded through the ice sheet, allowing inferences to be made about ice-surface elevation during the last glacial period (Håkansson et al., 2007; Rinterknecht et al., 2009; Roberts et al., 2008, 2009).

Conversely, elevation-dependent weathering differences can also result from burial of high-elevation surfaces by nonerosive, cold-based ice (Fig. 5), wherein highlands are covered by glacial ice for extended periods of time, but the ice is frozen to the bed and cannot perform erosion, leaving the landscape unaltered (Sugden, 1977, 1978; Sugden and Watts, 1977). This scenario could occur when ice cover over the lowlands is thick (allowing the base of the ice sheet to reach its pressure melting point), but ice cover over the highlands is thin (prohibiting the base of the ice sheet from reaching its pressure melting point). In this case, high-elevation samples have old single-nuclide minimum limiting exposure ages, poor agreement between bedrock and boulder samples, and $^{26}Al/^{10}Be$ ratios significantly below the constant exposure ratio that are indicative of burial (Fig. 5). Isotopic evidence for elevation-based erosion discrepancies has been found in Baffin Island, Canada (Bierman et al., 1999; Briner et al., 2003, 2006), Newfoundland, Canada (Gosse et al., 1993, 1995b), and Scotland (Phillips et al., 2006).

METHODS

Experimental Design

In the Upernavik region, we collected 20 bedrock and 13 boulder samples for analysis of in situ cosmogenic ^{10}Be and ^{26}Al. Samples were collected along a 100 km northwest-to-southeast transect extending from a nunatak ~2 km inside the present-day ice margin to the farthest outboard island (Table 1; Fig. 6). This transect is parallel to large fjords immediately to the north (Upernaviks Isfjord) and south (Laksefjorden) and roughly approximates paleo–ice-flow direction. Our sampling scheme, known as "dipstick sampling" (Stone et al., 2003), involved collecting samples at a variety of elevations at several locations along the transect normal to the ice margin. In Upernavik, we collected paired bedrock and boulder samples from a range of elevations (~20–1000 m above sea level [a.s.l.]) at each "dipstick." Such a sample distribution yields information about both vertical and horizontal variability in nuclide concentrations as well as differences between the exposure history of bedrock and overlying boulders, allowing us to make inferences about ice extent, subglacial erosion, and exposure history.

We present five different types of ages calculated with cosmogenic nuclides, all of which are minimum limits. For single-nuclide interpretations, we present both ^{10}Be and ^{26}Al ages, which are concordant in simple exposure scenarios. For paired-nuclide interpretations, we present modeled exposure durations, burial durations, and total history (the sum of exposure and burial durations). We correct the paired nuclide interpretations for Holocene exposure after the last deglaciation.

Field Methods

Wherever possible, we sampled bedrock and boulder pairs in close proximity, usually less than 10 m apart. We collected the uppermost several centimeters of material from the top surfaces of bedrock forms and perched boulders using a chisel and hammer (Table 1). We recorded latitude and longitude and elevation data with a handheld Garmin 12 global positioning system (GPS) that has a positional uncertainty of <10 m and an elevation uncertainty of <25 m.

Laboratory Methods

Samples were prepared as outlined in Corbett et al. (2011). We isolated quartz from the rock using a series of both physical and chemical

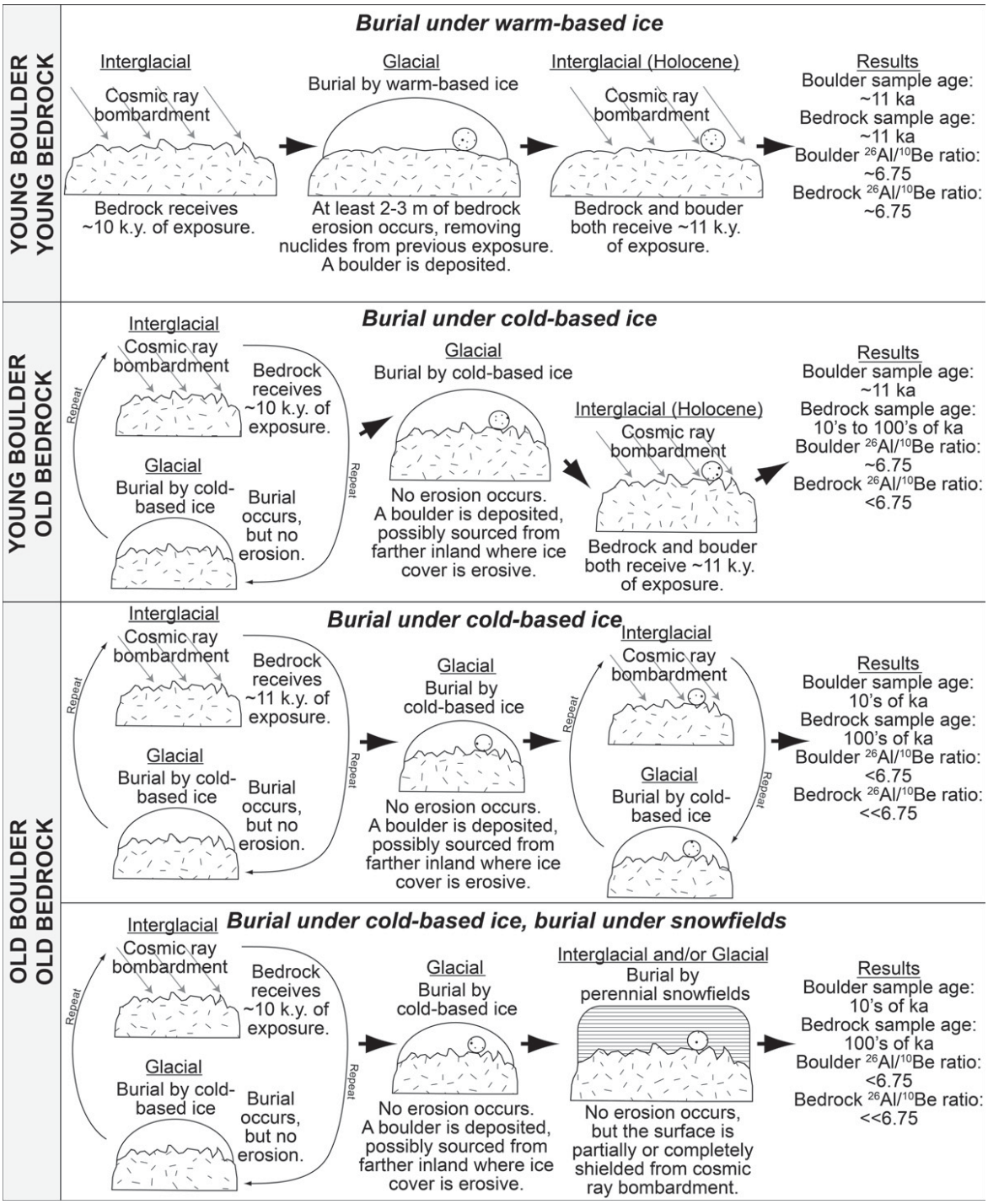

Figure 5. Illustration of bedrock-boulder minimum limiting age relationships and possible scenarios to explain them.

processes, and Be and Al from the quartz through a series of chemical processes. We used two different ^{9}Be carriers in the preparation of these samples: a commercial (SPEX) carrier for the first six samples and a low ^{10}Be/^{9}Be beryl carrier made at the University of Vermont for all subsequent samples. We added ~250 µg of ^{9}Be to each sample as a spike (see GSA Data Repository[1]).

In order to ensure that enough Al was present in the sample for isotopic analysis (2000 µg), we added commercial Al carrier (SPEX) when necessary. Immediately after quartz dissolution, we removed two aliquots representing ~6% of the material from each sample. We used these replicate aliquots to quantify the Al

[1]GSA Data Repository item 2013264, additional methodological information about sample isotopic analysis and retreat rate simulations, is available at http://www.geosociety.org/pubs/ft2013.htm or by request to editing@geosociety.org.

TABLE 1. SAMPLE LOCATION INFORMATION AND FIELD OBSERVATIONS

Dipstick number	Sample name	Sample type	Relative elevation*	Elevation (m a.s.l.)†	Latitude (°N)†	Longitude (°W)†	Rock type	Thickness (cm)§
Dipstick 1	GU091	Bedrock	Low	24	72.78189	56.58601	Granite	2
Offshore island	GU092	Boulder	Low	21	72.78199	56.58644	Granite	1.5
	GU093	Bedrock	High	91	72.73955	56.38520	Granite	2.5
Dipstick 2	GU094	Boulder	High	90	72.74016	56.38639	Granite	2
Offshore island	GU095	Bedrock	Low	20	72.74378	56.38154	Granite	3
	GU096	Bedrock	High	778	72.75386	55.87299	Granite	3
	GU097	Boulder	High	774	72.75388	55.87236	Granite	2
Dipstick 3	GU098	Bedrock	Mid	372	72.79260	55.93168	Granite	3
Fjord-dissected terrain	GU099	Boulder	Mid	366	72.79308	55.93311	Granite	1
	GU100	Bedrock	Low	74	72.81168	55.82623	Granite	1
	GU101	Boulder	Low	71	72.81164	55.82584	Granite	3
	GU102	Boulder	High	980	72.71763	55.47279	Foliated granite	2
	GU103	Bedrock	High	998	72.71811	55.47547	Granite	2
	GU106	Bedrock	High-mid	498	72.74086	55.55160	Granite	4
Dipstick 4	GU107	Boulder	High-mid	500	72.74085	55.55119	Foliated granite	2
Fjord-dissected terrain	GU104	Boulder	Low-mid	253	72.77333	55.50288	Granite	2
	GU105	Bedrock	Low-mid	270	72.77360	55.50378	Granite	1
	GU108	Bedrock	Low	33	72.78111	55.44319	Granite	2
	GU109	Boulder	Low	27	72.78024	55.44223	Granite	2
	GU110	Bedrock	High	745	72.66094	55.12159	Granite	1
	GU111	Bedrock	Mid	325	72.68163	55.02502	Granite	1
Dipstick 5	GU112	Boulder	Mid	325	72.68163	55.02502	Granite	1.5
Fjord-dissected terrain	GU113	Bedrock	Low	90	72.65953	54.98345	Granite	1
	GU114	Boulder	Low	91	72.65953	54.98345	Granodiorite	1.5
	GU001	Bedrock	High	603	72.53587	53.73338	Granite	3
Dipstick 6	GU002	Boulder	High	603	72.53587	53.73338	Granite	3
Ice-marginal terrain	GU006	Bedrock	Low	539	72.53920	53.73214	Granite	3.5
	GU017	Boulder	Low	539	72.53926	53.73214	Granite	1
	GU041	Bedrock	High	898	72.61509	53.58872	Granite	4
	GU042	Bedrock	High-mid	895	72.61546	53.59240	Granite	7
Dipstick 7	GU043	Bedrock	Mid	857	72.61594	53.59608	Granite	3
Nunatak	GU044	Bedrock	Low-mid	808	72.61743	53.59646	Granite	3
	GU045	Bedrock	Low	776	72.61870	53.59650	Granite	3

*Refers to the relative elevation of samples within each vertically oriented "dipstick."
†Elevations and locations were recorded in the field with a Garmin global positioning system (GPS) 12, in m above sea level (a.s.l.).
§Refers to the thickness of the slab that was collected for analysis.

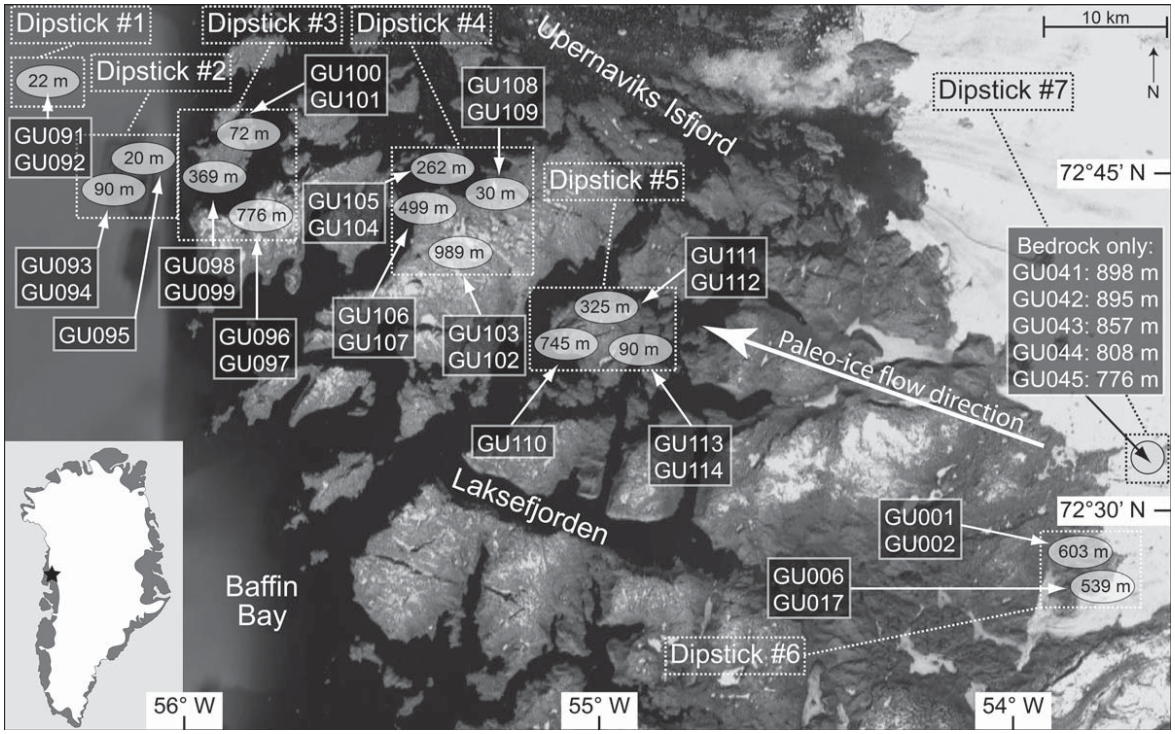

Figure 6. Study site map. Bedrock and boulder samples were collected along a 100-km-long northwest-southeast transect near Upernavik, Greenland, at seven different "dipsticks." Wherever possible, bedrock-boulder pairs were taken from a variety of elevations shown by gray ovals. Within each sample pair, the bedrock sample is listed first, followed by the boulder sample. In the few instances where boulders were not available, only the bedrock sample is listed. Satellite image is from the U.S. Geological Survey.

concentration of each sample through inductively coupled plasma–optical emission spectrometry (ICP-OES) using internal standardization (with Ga and Y) and measuring two different emission lines. The two measurements of sample Al concentration derived from these two aliquots were usually within 1%, and always within 3.5%, of each other. Measured Al concentrations of blanks were within 1% of expected Al concentrations based on the mass of ^{27}Al carrier that was added. Thus, the uncertainty in the ^{26}Al concentrations we report predominately reflects statistical limitations of accelerator mass spectrometry (AMS) measurements.

Isotopic Analysis

We measured isotopic ^{10}Be/^{9}Be and ^{26}Al/^{27}Al ratios by AMS at Lawrence Livermore National Laboratory (Perren et al., 2012; Rood et al., 2010). We analyzed all 33 samples for ^{10}Be, and normalized the samples to standard 07KNSTD3110, with a reported ^{10}Be/^{9}Be ratio of 2850×10^{-15} (Nishiizumi et al., 2007). Measured ^{10}Be/^{9}Be sample ratios ranged from 2.6×10^{-14} to 1.0×10^{-12} (see GSA Data Repository[1]), and ^{10}Be AMS measurement precisions, including propagated blank uncertainties, ranged from 1.9% to 5.4% (1σ). We subtracted process blank ratios (see GSA Data Repository[1]) from sample ratios and propagated blank uncertainties in quadrature.

After determining ^{10}Be concentrations and modeling minimum limiting exposure ages, we chose 20 samples to analyze for ^{26}Al. Sixteen of these 20 samples were chosen because of their old ^{10}Be ages (≥20 ka); for these samples, ^{26}Al analysis aids in distinguishing continuous exposure from complex exposure. Independent chronology from radiocarbon dating suggests that the Upernavik region was deglaciated ca. 10 cal k.a. B.P. (see "Study Site and Previous Work" section); therefore, we inferred that samples with ^{10}Be ages appreciably above ca. 10 ka likely do not have simple exposure histories. We also analyzed ^{26}Al in the two youngest bedrock samples (GU001 and GU098) and the two youngest boulder samples (GU002 and GU104); these four samples serve as a validation of simple exposure history in young samples and are herein referred to as "control" samples.

For ^{26}Al analysis, we normalized all samples to standard KNSTD10650, with a reported ^{26}Al/^{27}Al ratio of 10650×10^{-15} (Nishiizumi, 2004). Measured sample ^{26}Al/^{27}Al ratios ranged from 1.3×10^{-13} to 1.7×10^{-12} (see GSA Data Repository[1]), and AMS measurement precisions for ^{26}Al ranged from 2.4% to 12.8% (1σ). We subtracted process blank ratios (see GSA Data Repository[1]) from sample ratios and propagated blank uncertainties in quadrature.

Age Calculations

We calculated minimum limiting ^{10}Be and ^{26}Al exposure ages (Table 2) with the CRONUS Earth online exposure age calculator, developmental version 2.2, constants version 2.2 (Balco et al., 2008), under standard atmosphere. We used the regionally calibrated northeastern North American sea-level production rates of 3.93 ± 0.19 atoms g^{-1} yr^{-1} for ^{10}Be and 26.5 ± 1.3 atoms g^{-1} yr^{-1} for ^{26}Al (Balco et al., 2009), which are thought to be the most appropriate production rates for west Greenland (Briner et al., 2012). We also used the Lal/Stone constant production rate model and scaling scheme, which defines the variation in nuclide production rate with latitude and atmospheric pressure (Lal, 1991; Stone, 2000). In CRONUS, corrections were made for latitude, elevation, sample thickness (ranged from 1 to 7 cm), and sample density (assumed 2.7 g cm^{-3} for granite; Table 1).

We made no corrections for snow cover or till cover. Shielding by snow cover would lead to ^{10}Be or ^{26}Al age underestimates (Schildgen et al., 2005); however, seasonal snow-cover effects at our sample sites are likely minimal. Using data from a weather station in the town of Upernavik (www.weather-and-climate.com), we determined that mean temperatures are below freezing for 8 months of the year (October through May) and that ~140 mm of snow water equivalent falls during this time at a rate of ~7–35 mm/month. Assuming that winter precipitation was added in monthly increments, that the density of settled seasonal snow is 0.3 g cm^{-3}, and that no melting or sublimation occurred until June, shielding calculations (Gosse and Phillips, 2001) suggest that reported exposure ages could underestimate the true age by no more than 2%. This calculation is likely a significant overestimate because the areas we sampled are windswept and exposed during winter months and because we did not account for snow loss during the winter. However, snowfall patterns during the Pleistocene were likely different than those indicated by the modern weather data.

We made no corrections for postexposure erosion of rock surfaces, which can lead to cosmogenic exposure age underestimates. Although boulders at low elevations did not preserve striations, the surfaces we sampled were glacially abraded (Fig. 2), indicating at most a few centimeters of erosion after the sample sites were exposed by deglaciation. Field observations suggest that subaerial erosion has removed mass from rock surfaces at high elevations (Fig. 3); however, because we have no reliable erosion rate estimates for these surfaces, we cannot correct cosmogenic ages for erosion. Thus, all reported ages for high- and low-elevation surfaces represent minimum limits.

Reported uncertainties reflect AMS errors only, which we refer to as "internal." Because we are primarily interested in investigating relationships between samples within the data set (i.e., a bedrock sample vs. its paired boulder), we use internal uncertainties in our data analysis. Additional uncertainties are introduced in relation to nuclide production rates, elevation corrections, and latitude corrections when comparing the ages in this study to ages in other data sets. However, we can expect errors in calibration and correction to be correlated and thus to affect all samples similarly because our samples come from a geographically limited region.

Data Reduction and Interpretation

Single-nuclide minimum limiting ^{10}Be and ^{26}Al exposure ages for each sample were calculated with the CRONUS Earth online calculator (Balco et al., 2008). We also considered both nuclides together to present minimum limiting exposure and burial durations (Bierman et al., 1999). Elevation-scaled production rates for our samples range from 4.37 to 10.8 atoms g^{-1} yr^{-1} for ^{10}Be and from 29.5 to 72.6 atoms g^{-1} yr^{-1} for ^{26}Al. We assume a ^{26}Al/^{10}Be production ratio of 6.75 (Balco et al., 2009), a ^{10}Be half-life of 1.36×10^{6} yr (Nishiizumi et al., 2007), and a ^{26}Al half-life of 7.05×10^{5} yr (Nishiizumi, 2004). Calculations involving burial assume complete burial with no nuclide production.

We compare our results to a similar study (Bierman et al., 1999) conducted in Baffin Island, Canada, because of its close proximity and similar latitude, elevation, and sampling strategy. We recalculated the production rates for samples presented by Bierman et al. (1999) in CRONUS using the northeastern North American production rate, and remodeled minimum limiting exposure and burial durations and total histories using updated decay constants so that the data from Upernavik and Baffin Island are directly comparable.

A correction for Holocene exposure was done as part of the two-isotope analysis. We chose a value of 11.3 k.y. for the Holocene exposure duration of Upernavik samples (see "Postglacial Ice Retreat" section of the Discussion) and 9.5 k.y. for Baffin Island samples based on measurements of deglaciation age from Briner et al. (2009). We normalized the elevation-scaled production rates in CRONUS to the sea-level production rate, calculated the inventory of ^{10}Be and ^{26}Al accumulated during the past 11.3 and 9.5 k.y., respectively, and subtracted these values from the total concentrations before proceeding with other calculations. Implementing

Geological Society of America Bulletin, published online on 23 July 2013 as doi:10.1130/B30813.1

TABLE 2. SAMPLE ISOTOPIC INFORMATION AND AGE CALCULATIONS

Sample name	Sample type	Measured values*		Holocene-corrected and elevation-normalized values			Single-nuclide interpretation (minimum limiting)		Paired-nuclide interpretation (minimum limiting)		
		^{10}Be (atoms g^{-1})	^{26}Al (atoms g^{-1})	^{10}Be (atoms g^{-1})	^{26}Al (atoms g^{-1})	^{26}Al/^{10}Be ratio	^{10}Be age†	^{26}Al age†	Exposure duration (k.y.)§	Burial duration (k.y.)§	Total history (k.y.)§
GU091	Bedrock	6.98×10^4	–	–	–	–	16.4	–	–	–	–
GU092	Boulder	6.19×10^4	–	–	–	–	14.5	–	–	–	–
GU093	Bedrock	7.29×10^4	–	–	–	–	15.9	–	–	–	–
GU094	Boulder	5.17×10^4	–	–	–	–	11.3	–	–	–	–
GU095	Bedrock	6.63×10^4	–	–	–	–	15.7	–	–	–	–
GU096	Bedrock	9.09×10^5	5.22×10^6	3.64×10^5	2.05×10^6	5.6 ± 0.2	104	89.4	112	323	435
GU097	Boulder	1.77×10^5	1.19×10^6	3.47×10^4	2.32×10^5	6.7 ± 0.4	19.7	19.6	9	15	24
GU098	Bedrock	8.38×10^4	5.90×10^5	5.57×10^4	3.93×10^5	7.0 ± 0.6	13.7	14.3	14	0	14
GU099	Boulder	7.11×10^4	–	–	–	–	11.5	–	–	–	–
GU100	Bedrock	1.01×10^5	7.26×10^5	4.65×10^4	3.54×10^5	7.6 ± 0.4	22.3	23.7	10	0	10
GU101	Boulder	5.03×10^4	–	–	–	–	11.3	–	–	–	–
GU102	Boulder	4.90×10^5	2.70×10^6	1.38×10^5	7.03×10^5	5.1 ± 0.6	45.7	37.3	47	557	604
GU103	Bedrock	9.07×10^5	5.17×10^6	2.86×10^5	1.59×10^6	5.5 ± 0.2	83.9	71.5	90	365	454
GU106	Bedrock	2.28×10^5	1.47×10^6	9.06×10^4	5.72×10^5	6.3 ± 0.3	33.5	32.1	25	127	152
GU107	Boulder	9.79×10^4	–	–	–	–	14.1	–	–	–	–
GU104	Boulder	6.03×10^4	4.31×10^5	4.50×10^4	3.22×10^5	7.2 ± 0.9	11.1	11.7	11	0	11
GU105	Bedrock	2.35×10^5	1.50×10^6	1.27×10^5	7.95×10^5	6.3 ± 0.3	42.4	40.2	35	140	175
GU108	Bedrock	8.55×10^4	–	–	–	–	19.9	–	–	–	–
GU109	Boulder	6.98×10^4	–	–	–	–	16.4	–	–	–	–
GU110	Bedrock	5.67×10^5	2.67×10^6	2.14×10^5	9.20×10^5	4.3 ± 0.2	65.2	45.4	88	901	989
GU111	Bedrock	4.26×10^5	2.37×10^6	2.49×10^5	1.33×10^6	5.3 ± 0.2	73.3	60.6	81	445	526
GU112	Boulder	1.21×10^5	7.74×10^5	3.92×10^4	2.35×10^5	6.0 ± 0.3	20.6	19.5	11	236	247
GU113	Bedrock	2.37×10^5	1.52×10^6	1.66×10^5	1.05×10^6	6.3 ± 0.3	51.9	49.4	45	116	161
GU114	Boulder	5.58×10^4	–	–	–	–	12.1	–	–	–	–
GU001	Bedrock	1.03×10^5	6.79×10^5	5.48×10^4	3.62×10^5	6.6 ± 0.4	13.6	13.2	14	38	52
GU002	Boulder	8.06×10^4	5.59×10^5	4.29×10^4	2.98×10^5	6.9 ± 0.6	10.6	10.9	11	0	11
GU006	Bedrock	1.18×10^5	–	–	–	–	16.6	–	–	–	–
GU017	Boulder	9.32×10^4	–	–	–	–	12.9	–	–	–	–
GU041	Bedrock	7.83×10^5	4.38×10^6	2.75×10^5	1.49×10^6	5.4 ± 0.2	80.9	67.6	88	415	503
GU042	Bedrock	5.02×10^5	2.98×10^6	1.66×10^5	9.54×10^5	5.7 ± 0.2	52.9	46.8	50	316	366
GU043	Bedrock	4.95×10^5	3.13×10^6	1.64×10^5	1.02×10^6	6.2 ± 0.2	52.3	49.2	46	153	199
GU044	Bedrock	5.79×10^5	3.55×10^6	2.10×10^5	1.26×10^6	6.0 ± 0.2	64.1	58.7	61	213	274
GU045	Bedrock	3.82×10^5	2.12×10^6	1.29×10^5	6.62×10^5	5.1 ± 0.2	43.3	35.6	43	542	585

*Ratio uncertainties for ^{10}Be/^{9}Be and ^{26}Al/^{27}Al are included in the GSA Data Repository.

†Ages were calculated using the northeastern North American production rates of 3.93 ± 0.19 atoms g^{-1} yr^{-1} for ^{10}Be and 26.5 ± 1.3 atoms g^{-1} yr^{-1} for ^{26}Al (Balco et al., 2009) and the Lal (1991)/Stone (2000) scaling scheme in CRONUS. Ages have been scaled for elevation, sample density, sample thickness, latitude, and longitude.

§Calculated with the Holocene-corrected and elevation-normalized ^{10}Be and ^{26}Al concentrations.

this Holocene correction shifts samples leftward and downward on the two-isotope plot, yielding shorter minimum limiting exposure durations and longer minimum burial durations. Although we used the best available data to designate a Holocene exposure duration, this choice introduces additional uncertainty to the two-isotope calculations. Using a slightly different Holocene exposure duration (~1–2 k.y. in either direction) would yield minimum limiting exposure durations differing by several thousand years and minimum limiting burial durations differing by several tens of thousands of years.

Retreat Rate Simulations

To estimate the rate of latest Pleistocene ice-sheet retreat along the sample transect, we considered only the youngest overlapping boulder sample ages ($n = 6$), assuming that they inherited no nuclides from prior periods of exposure. We systematically simulated potential linear retreat patterns taking into account the location of each sample and uncertainty of each age measurement (see GSA Data Repository[1]) in order to calculate a statistically most likely retreat rate.

RESULTS

Data Overview and Minimum Limiting Exposure Ages

For the 33 samples in the data set, measured ^{10}Be concentrations range from 5.0×10^4 to 9.1×10^5 atoms g^{-1} (Table 2). For the 20 samples on which ^{26}Al analysis was conducted, ^{26}Al concentrations range from 4.3×10^5 to 5.2×10^6 atoms g^{-1} (Table 2). Single-nuclide minimum limiting exposure ages range from 10.6 to 104 ka for ^{10}Be, and from 10.9 to 89.4 ka for ^{26}Al (Fig. 7). Comparison of the two single-isotope concentrations for an individual sample yields a strong correlation ($r^2 = 0.99$; Fig. 8). In general, ^{10}Be and ^{26}Al single-nuclide concentrations are more similar for samples with shorter exposure times, and the ^{10}Be/^{26}Al ratio is close to the production ratio of ~6.75. For longer exposure times, the concentration of ^{10}Be increases relative to the concentration of ^{26}Al, and the ^{10}Be/^{26}Al ratio decreases below 6.75.

The ^{26}Al/^{10}Be ratios range from ~4.3 to 7.6 (Fig. 9). The four "control" samples used to test for consistency with the assumed ^{26}Al/^{10}Be production ratio of 6.75 (GU001, GU002, GU098, and GU104) fall along the constant exposure path (see "Using Cosmogenic Nuclides to Understand Glacial Exposure and Erosion" section) and have an average ^{26}Al/^{10}Be ratio of 6.9 ± 0.2 (average ± 1 standard deviation [SD]), which is indistinguishable from the production

ratio within uncertainty. Of the remaining 16 samples for which ^{26}Al was measured, two (GU097 and GU100) have ^{26}Al/^{10}Be ratios that overlap the constant exposure path within uncertainty. The other 14 samples fall below the region of constant exposure and/or steady erosion; their ^{26}Al/^{10}Be ratios can be explained by varying lengths of burial after at least one period of surface exposure or by exposure under a thin cover of sediment or ice.

Bedrock and Boulder Comparisons

There is a pronounced contrast between bedrock and boulder nuclide concentrations and calculated minimum limiting exposure ages. Within all 13 sample pairs, the bedrock sample has a higher concentration of ^{10}Be than the boulder sample by more than 1σ, considering analytical uncertainties. Bedrock samples contain, on average, ~2.3 times as much ^{10}Be as corresponding boulder samples, although this value varies from ~1.1 to 5.1 times. Corresponding bedrock and boulder sample pairs have dissimilar minimum limiting ^{10}Be exposure ages and do not have a 1:1 relationship (r^2 = 0.41; Fig. 10). A repeated measures *t*-test verifies that there is a statistically significant difference when minimum limiting bedrock and boulder ages are considered in a paired comparison (p = 0.007). Considering bedrock and boulder samples in two distinct populations also results in nonoverlapping population distributions (Fig. 11); an independent samples *t*-test indicates that there is a statistically significant difference between the populations (p = 0.022).

Spatial Variability

Minimum limiting sample ages vary in the vertical dimension; both bedrock (R^2 = 0.43; n = 20) and boulder (R^2 = 0.41; n = 13) minimum limiting ^{10}Be ages increase with elevation (Fig. 12). A one-way analysis of variance (ANOVA) shows that the minimum limiting bedrock sample ^{10}Be age has a weakly significant relationship with elevation (p = 0.051), using the relative elevation of each sample within its own dipstick (Table 1). The same test performed on boulder samples shows that the minimum limiting ^{10}Be age has a more significant relationship with elevation (p = 0.01). Spatial variability is not detectable in the horizontal dimension; there is no relationship between minimum limiting sample age and distance along the 100-km-long sample transect.

Five bedrock samples from the nunatak yielded minimum limiting ^{10}Be ages of 43.3–80.9 ka, and minimum limiting ^{26}Al ages of 35.6–67.6 ka. The lowest-elevation nunatak sample has the youngest minimum limiting single-nuclide ages (43.3 and 35.6 ka for ^{10}Be and ^{26}Al, respectively), while the highest-elevation nunatak sample has the oldest minimum limiting single-nuclide ages (80.9 and 67.6 ka for ^{10}Be and ^{26}Al, respectively). Calculated ^{26}Al/^{10}Be ratios range from 5.1 to 6.2, overlap within uncertainty, and all fall below the constant exposure path. The two-isotope minimum limiting exposure duration is least for the lowest-elevation nunatak sample (43 k.y.) and greatest for the highest-elevation nunatak sample (88 k.y.).

DISCUSSION

Results from this study suggest that the Upernavik landscape has a long and complex glacial history. The presence of young, Holocene-age boulder samples at low elevations demonstrates that at least some surfaces are free of cosmogenic nuclides inherited from previous periods of exposure. However, the majority of the data set has older (up to ca. 100 ka) minimum limiting ^{10}Be and ^{26}Al ages and therefore does not provide insight about the timing of the latest Pleistocene deglaciation. Using dual-isotope analysis and correcting for the past 11.3 k.y. of Holocene re-exposure, calculated minimum limiting exposure durations range up to 112 k.y., burial durations range up to 900 k.y., and total histories are as high as 990 k.y., all of which are indicative of a landscape that has been buried

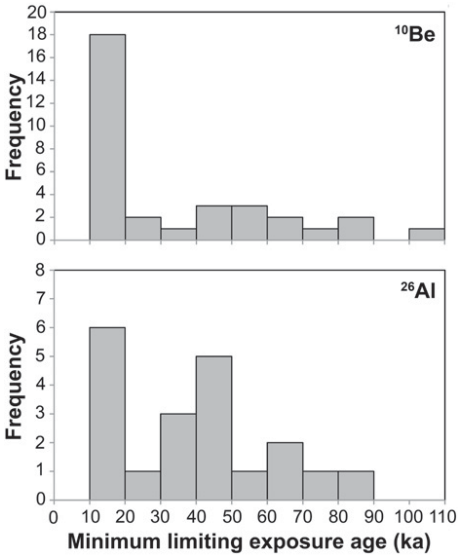

Figure 7. Top: Histogram of minimum limiting ^{10}Be exposure ages for all 20 bedrock and 13 boulder samples. Bottom: Histogram of minimum limiting ^{26}Al exposure ages for the 15 bedrock and five boulder samples on which Al analysis was performed.

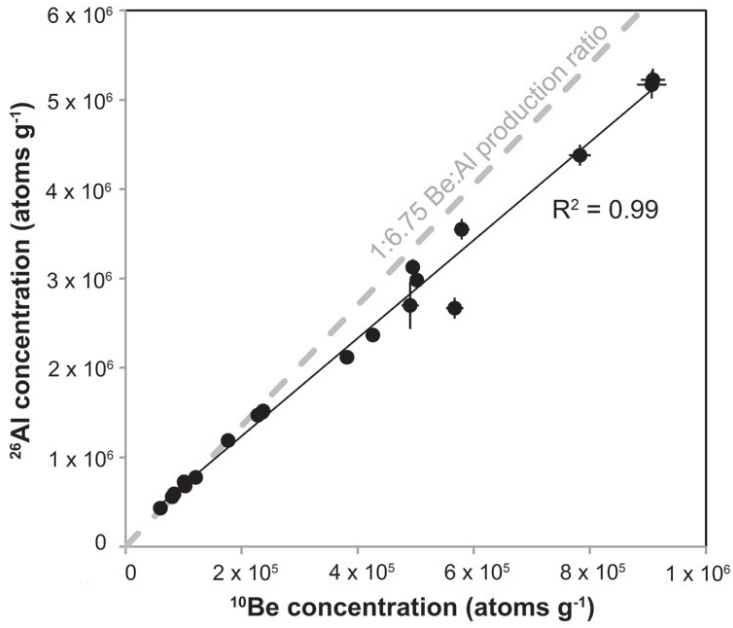

Figure 8. Correlation of ^{10}Be and ^{26}Al concentrations for all samples with dual isotope analysis (n = 20). Error bars show 1σ internal error; in most cases, error bars are smaller than the data points. The gray dashed line represents the 1:6.75 (Be:Al) production ratio.

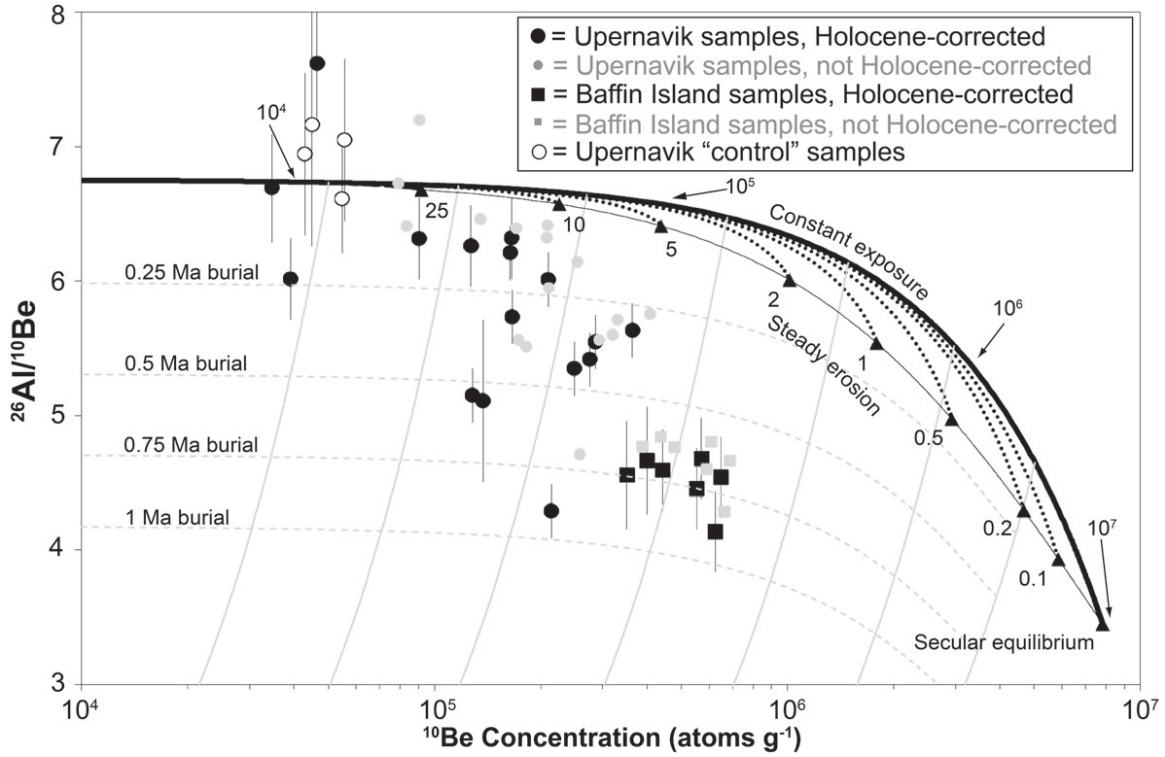

Figure 9. ^{26}Al/^{10}Be ratios plotted against ^{10}Be concentrations for 15 bedrock and five boulder samples from Upernavik, as well as seven comparable samples from Baffin Island, Canada (recalculated from Bierman et al., 1999). Exposure durations (in yr) are shown along the thick black "constant exposure" path. Erosion rates, in m m.y.$^{-1}$, are shown along the bottom of the "steady erosion" envelope. Individual erosion paths for selected erosion rates are shown with black dotted lines. Burial paths are shown with thin gray lines, and burial isochrones are shown with thin gray dashed lines. Error bars show 1σ internal error.

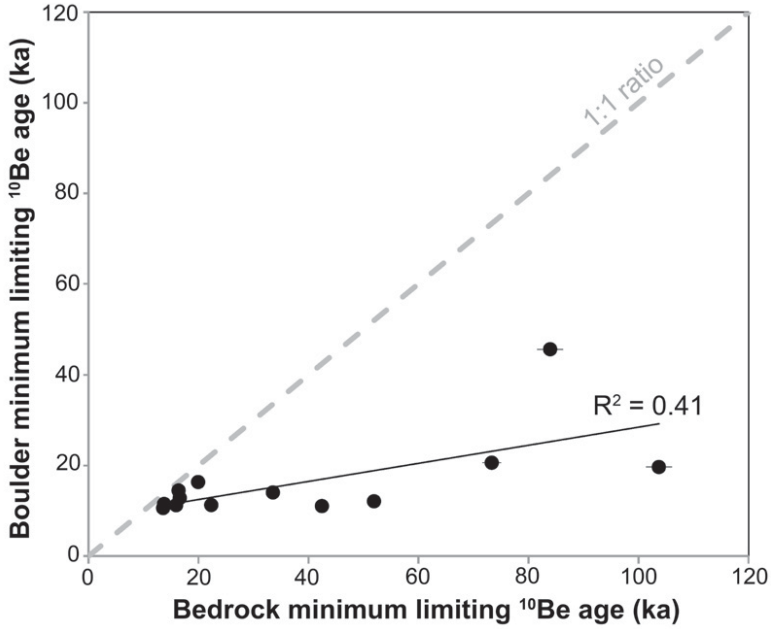

Figure 10. Comparison of bedrock and boulder sample ages shown by a correlation of minimum limiting ^{10}Be ages for 13 sample pairs. Error bars show 1σ internal error; in most cases, error bars are smaller than the data points. The gray dashed line represents a 1:1 relationship between ages.

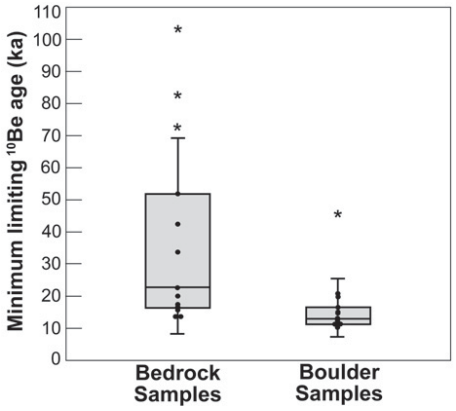

Figure 11. Comparison of minimum limiting bedrock and boulder sample age populations shown by box and whisker plots (bedrock, n = 20; boulders n = 13). The box encloses the area between the first and third quartiles, and the horizontal line represents the median. Whiskers show one standard deviation. Samples that lie outside one standard deviation from the mean are shown with an asterisk; all other samples are shown with dots.

for long periods by ice that performed little if any erosion.

Glacial Period Ice Thickness and Extent

The presence of erratic boulders on upland surfaces demonstrates that ice during glacial periods in the Upernavik region covered the highest peaks (~1000 m a.s.l.) at least once since the initiation of glaciation on Greenland, which occurred during the late Pliocene (Bartoli et al., 2005). These glacially transported boulders, which do not match the local bedrock type (e.g., GU102, boulder, foliated granite; and GU103, bedrock, unfoliated granite), suggest that the Upernavik uplands were once covered by the Greenland Ice Sheet rather than just by local ice caps or ice fields. Similar observation of mismatched bedrock-boulder lithologies has been made in Melville Bugt, ~300 km to the north (Kelly, 1980), indicating that Greenland Ice Sheet cover of upland surfaces was regional in nature.

Deglaciation ages of the farthest outboard samples show that ice extended at least ~100 km northwest of the present-day ice-sheet margin, providing a minimum estimate for the spatial extent of ice cover that was lost during the last deglaciation. Several of these samples came from low elevations (e.g., GU091 at 24 m and GU092 at 21 m), and their ages could represent marine emergence rather than deglaciation. However, a compilation of data from around Greenland's coast shows that relative sea level in the Upernavik region was only 0–20 m above modern sea level during the early Holocene following deglaciation (Funder and Hansen, 1996), placing Upernavik in the zone of least isostatic rebound around Greenland. Long et al. (2006) found that the marine limit could be approximated by the lowest elevation of perched boulders; since we sampled perched boulders even at the low elevations in Upernavik, the boulder samples in question are likely to have been above the local marine limit. Additionally, there is no indication in the data that the samples close to the marine limit are systematically younger than those at higher elevations. Even if these lowest samples were submerged, the rate of land surface rebound during the early Holocene was so rapid (Ten Brink, 1974) that the effect of initial submergence on their exposure ages would be insignificant.

Isotope Inheritance and Subglacial Erosion Efficiency

This data set demonstrates that cosmogenic isotopes inherited from prior periods of exposure are present in most of the rock surfaces near Upernavik. The old minimum limiting ^{10}Be ages, positive skew of the data (Fig. 7), disagreement between bedrock and boulder samples (Figs. 10 and 11), and long exposure durations modeled from two-isotope data (Table 2) suggest that most samples contain more ^{10}Be than could have accumulated during the Holocene. This excess ^{10}Be is inherited from previous periods of exposure, when the climate warmed and bedrock surfaces and perched boulders were exposed. Such exposure would have occurred during many previous interglacial periods throughout the Quaternary when global ice volume was low (Lisiecki and Raymo, 2005).

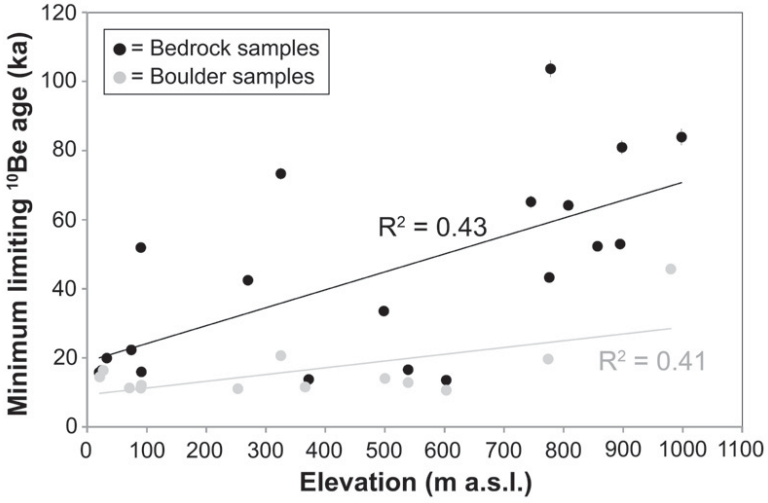

Figure 12. Correlation of minimum limiting sample age and elevation for bedrock samples (n = 20) and boulder samples (n = 13). Error bars show 1σ internal error; in most cases, error bars are smaller than the data points.

Upland surfaces show the longest durations of burial. The highest-elevation bedrock samples (GU096, 778 m; GU103, 998 m; and GU110, 745 m) all have ^{26}Al/^{10}Be ratios less than ~5.75, indicating that burial occurred at least once after initial exposure. The average minimum burial duration for samples showing burial is 324 ± 226 k.y. (1SD, Holocene-corrected); because glacial periods last roughly ~100 k.y., these long burial durations demonstrate that high-elevation surfaces have been repeatedly covered by nonerosive ice or snow. Perennial snowfields may explain some of this burial signal; assuming a settled snow density of 0.4 g cm^{-3}, the snowpack would need to reach a depth of ~10 m to effectively shield rock surfaces from spallation-induced nuclide production. Complete burial by cold-based glacial ice or thick snowfields, or partial burial by thin snowfields or till, could have occurred following initial exposure (Fig. 5). However, the presence of discordant bedrock and boulder ages indicates that the boulders were emplaced at some point after the initial exposure and burial of the bedrock; thus, the most likely explanation for mismatched minimum limiting bedrock-boulder ages is burial by cold-based ice at least once after initial exposure (Fig. 5).

The presence of inherited ^{10}Be indicates that subglacial erosion rates were low, and that glacial ice was not capable of removing all ^{10}Be inherited from preceding interglacial periods (Fig. 5). Furthermore, the relationship between minimum limiting sample age and elevation (Fig. 12) suggests that glacial ice removed more material from low elevations than it did from high elevations (Briner et al., 2006). This interpretation is consistent with field observations. Low-elevation areas display streamlined landforms indicative of glacial erosion (Fig. 2), while high-elevation areas preserve evidence of extended surface weathering (Fig. 3). Elevation-related erosion intensity is likely caused by the relationship between ice thickness and subglacial temperatures; low-elevation land surfaces were covered by thicker ice, at or near the pressure melting point, which would have been more erosive than the thinner cold-based ice that covered high-elevation surfaces.

While elevation-related erosion intensity governs the overall trend of sample ages with elevation, there is still noise in the data. The sample with the longest modeled total history (GU110, 989 ka) is from an elevation of 745 m a.s.l.; there are numerous higher-elevation samples with shorter total histories. The five samples from the nunatak (dipstick 7; Fig. 6) do not show a correlation between elevation and modeled total history, maybe because all of the samples have similar elevations (within 100 m),

and ice erosivity did not vary appreciably over this thickness. Deviations from the trend of increasing sample age with elevation likely arise from local variability in glacial erosive power, differences of subaerial erosion during interglacial periods, rock hardness, small shielding effects, and the possibility that ice lingered longer at lower elevations.

Some boulder samples also preserve inherited ^{10}Be, although not as much as bedrock samples. Boulders were quarried farther inland and then transported coastward to their present locations. They may have originated from inheritance-bearing outcrops, which were originally covered by nonerosive ice but subsequently covered by erosive ice capable of quarrying. They also may have been plucked from outcrops far inland from the coast, where ice is thicker and more likely warm-based, before being transported into a zone of cold-based ice around the margin. There is appreciable spread in the minimum limiting ^{10}Be ages of boulder samples (ranging fourfold, from 10.6 to 45.7 ka), possibly documenting a variety of different sources, erosion mechanisms, or transport histories.

The low efficiency of subglacial erosion we infer in Upernavik is consistent with findings in other high-latitude areas. Inheritance of cosmogenic nuclides from prior periods of exposure has been documented in Greenland (Goehring et al., 2010; Håkansson et al., 2008; Kelly et al., 2008), the Canadian Arctic (Bierman et al., 1999; Briner et al., 2003; Marquette et al., 2004), Scandinavia (Goehring et al., 2008; Harbor et al., 2006; Stroeven et al., 2002b), and Antarctica (Lilly et al., 2010; Sugden et al., 2005). These regions are characterized by cold mean annual temperatures that would favor the existence of an ice sheet partially frozen to the bed.

However, not all high-latitude regions have cold-based ice. The presence of inherited nuclides in Upernavik differs notably from the Jakobshavn Isbræ region, 500 km south. There, no inheritance of cosmogenic isotopes from prior periods of exposure was detected, regardless of sample type or elevation (Corbett et al., 2011). The lack of inheritance there may reflect thick ice in Jakobshavn Isbræ, which eroded sufficient material from bedrock outcrops to remove any inherited isotopes. The pronounced contrast between inferred subglacial erosion efficiency in Upernavik (low) and Jakobshavn (high) indicates that landscapes buried by ice in or around large ice streams likely experience more efficient erosion than those buried by thinner, more slowly flowing ice. Climate probably also plays a role, since the mean annual temperature in Upernavik is ~2.5 °C colder than in Ilulissat (www.weather-and-climate.com). Subglacial erosion efficiency, therefore, may be controlled by local factors such as ice thickness and ice-flow velocity, as well as larger-scale regional climatic conditions.

Landscape Evolution

Parts of the Upernavik landscape have been preserved through multiple glacial-interglacial cycles. High-elevation bedrock surfaces have minimum limiting total histories of hundreds of thousands of years, suggesting that the highlands were minimally altered through repeated burial by glacial ice. Burial dominates the landscape history; most high-elevation surfaces have minimum limiting burial durations of ~300–500 k.y. and minimum limiting total histories of ~500–600 k.y., suggesting that these surfaces experienced burial with limited erosion ~75% of the time.

The high-elevation surfaces on Baffin Island, ~600 km to the west, have longer minimum limiting exposure durations, burial durations, and total histories than similar surfaces in Upernavik (using recalculated data from Bierman et al., 1999; Figs. 9 and 13). On average, bedrock surfaces on Baffin Island record total histories almost two times as long (~900 k.y.) as those in Upernavik. However, despite differences in duration, the relative role of burial appears to be similar between Baffin Island and Upernavik. The Baffin Island samples have a burial to total history ratio of 0.79 ± 0.04 (average ± 1 SD); the Upernavik samples (taking into account only bedrock samples at elevations >600 m in order to match the Baffin Island data set) have a burial to total history ratio of 0.83 ± 0.07 (average ± 1 SD). Thus, despite recording different durations of Quaternary history, both upland surfaces have experienced burial for the same portion of time. The value of ~0.8 is likely a reflection of the fraction of time represented by glacial periods and expanded ice volume throughout the latter part of the Quaternary.

In Upernavik, the presence of cosmogenic nuclide inheritance in bedrock samples deep within fjords raises the question of how the fjords formed, if not by glacial erosion. Given that glaciers can form a recognizable U-shaped valley from a preexisting V-shaped valley in as little as 10,000 yr (Harbor, 1992), even one or two glacial periods of thick, highly erosive ice could cause significant reshaping of the landscape. However, it is probable that ice cover in Upernavik has been cold-based for the majority of the Quaternary, and has not been a major player in landscape development. More likely, the origin of these fjords is tectonic, and thus glacial activity has been only a recent overprint upon an older structure (England, 1987; Glasser and Ghiglione, 2009; Swift et al., 2008). Bonow et al. (2007) suggested that uplift of the west Greenland coast occurred during the late Miocene and Pliocene, as seafloor spreading was initiated in the North Atlantic. Continued erosion created planar surfaces, which were uplifted to create the low-relief highlands visible in western Greenland today. Fluvial erosion incised these surfaces as rivers responded to changing base levels, creating a landscape of planar highlands dissected by deep valleys (Bonow et al., 2007). Repeated burial by cold-based, nonerosive glacial ice during the Quaternary has likely done little to modify this landscape; this implies that the fjords in Upernavik may be relict features, preserved from the Miocene or Pliocene (Bonow et al., 2007).

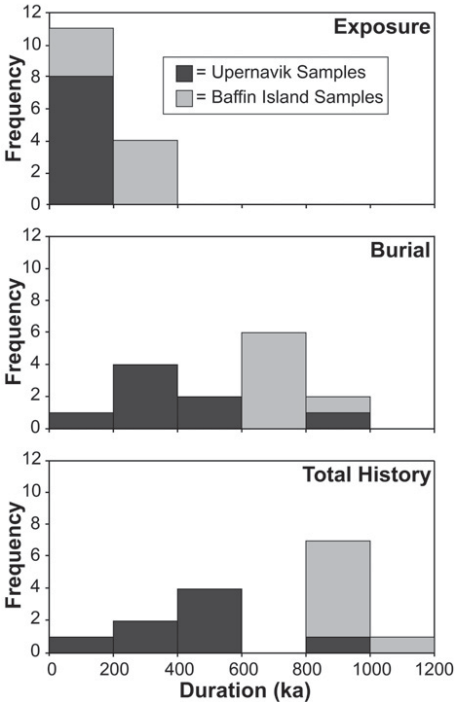

Figure 13. Histograms of minimum limiting exposure durations, burial durations, and total histories from highlands in Upernavik, Greenland (this study), and Baffin Island, Canada (recalculated from Bierman et al., 1999). The Upernavik data include only bedrock samples from elevations >600 m in order to be comparable to the samples from Baffin Island. All samples have been corrected for 11.3 k.y. (Upernavik) or 9.5 k.y. (Baffin) of Holocene exposure and scaled for elevation-based differences in production rates.

Geological Society of America Bulletin, published online on 23 July 2013 as doi:10.1130/B30813.1

Postglacial Ice Retreat

Determining the timing of ice retreat in the deep fjords after the last glacial period is possible because a small subset of the samples appear to have simple exposure histories. The six youngest boulder samples have overlapping ^{10}Be ages of 11.3 ± 0.5 ka, and we interpret this to be the best estimate for the deglaciation of the exposed land surface near Upernavik. This reported age is the mean exposure age ± one standard deviation; systematic uncertainties in production rate would shift the central tendency slightly but not change the relationship between samples. This cosmogenic estimate for deglaciation is consistent with other estimates of minimum limiting deglaciation age from radiocarbon dating discussed in the "Study Site and Previous Work" section.

The low-elevation boulder samples show no trend in age along the 100-km-long sample transect, suggesting that significant lateral retreat of the ice margin (~100 km) likely occurred within several hundred years. The modeled statistical maximum likelihood ice retreat rate was ~120 m yr^{-1}, with possible rates as low as 80 m yr^{-1} and as high as 240 m yr^{-1} (1 SD). Rapid retreat of the ice margin was likely facilitated by calving, since ice in the Upernavik region would have been largely marine-based due to local topography, which consists of small islands separated by large fjords (Fig. 6). These results support the proposition that areas of marine-based ice can undergo periods of rapid collapse in a warming climate (England, 1976; Mangerud et al., 2013; Straneo et al., 2012).

The retreat of the ice-sheet margin in Upernavik shows a pattern of retreat similar to that of the Helheim Glacier in southeastern Greenland. There, Hughes et al. (2012) used ^{10}Be exposure dating on bedrock and boulder samples and determined that samples collected along the entire length of the ~60 km fjord had indistinguishable exposure ages within two SD. The mean age of boulders indicates that retreat took place very quickly at 10.8 ± 0.3 ka. The timing of rapid ice loss from Helheim Fjord (Hughes et al., 2012) overlaps with the estimate of rapid ice loss from Upernavik presented here (11.3 ± 0.5 ka) and suggests that the episode of abrupt early Holocene retreat seen in Upernavik is not spatially restricted. The rapid episode of glacial retreat documented in both Upernavik and in Helheim Fjord appears to have occurred earlier than retreat in Ilulissat, 500 km to the south, where the present-day coastline did not become ice free until ca. 10.3 k.y. B.P. (Corbett et al., 2011; Young et al., 2011).

The rate of ice-margin retreat in Upernavik is similar to some but higher than many estimates of retreat rates for large bodies of ice from the same time period (see Fig. 9 in Corbett et al., 2011). In Ilulissat, 500 km to the south, calculated rates of ice-margin retreat were ~100–110 m yr^{-1} through Jakobshavn Isfjord, its tributary fjord, and its adjacent bay (Corbett et al., 2011; Long and Roberts, 2003; Long et al., 2006; Young et al., 2011). In Sisimiut Fjord, central western Greenland, retreat rates were ~20–50 m yr^{-1} (Rinterknecht et al., 2009). In North America, retreat rates of ~60 m yr^{-1} were calculated for Sam Ford Fjord on Baffin Island (Briner et al., 2009). Ice retreat rate, therefore, appears to be controlled by local and regional factors.

Rapid ice loss from the Upernavik area ca. 11.3 ± 0.5 ka may have been driven by external climate forcing (Fig. 14). Oxygen isotope ratios from the Greenland Ice Sheet Project 2 (GISP2) ice core (Stuiver and Grootes, 2000) and from the Greenland Ice Core Project (GRIP) and Dye3 ices cores (Dahl-Jensen et al., 1998) show that this time period was characterized by rapid warming. This warming may have coincided with the end of the Younger Dryas cold event (Alley, 2000; Taylor et al., 1993), which is thought to have occurred rapidly in the Arctic over several abrupt subdecadal pulses at 11,645 ± 200 and 11,612 ± 200 yr B.P. (Taylor et al., 1997). However, any causal relationship is speculative because only six of the samples appear to record deglaciation age, and because the average deglaciation age of the Upernavik fjords has an uncertainty of 500 yr (1 SD).

CONCLUSIONS

Analysis of ^{10}Be and ^{26}Al in paired bedrock and boulder samples near Upernavik, northwest Greenland, reveals a complex landscape history. Bedrock and boulder samples have discordant ^{10}Be and ^{26}Al minimum limiting ages, suggesting that nuclides inherited from previous periods of exposure are present. High-elevation surfaces have old single-nuclide minimum limiting exposure ages and record at least several hundred thousand years of burial after initial exposure. These surfaces, which exhibit pronounced surface weathering features, have likely been preserved under nonerosive, cold-based ice or perennial snowfields over the course of numerous glacial cycles. The existence of these relict surfaces suggests that, despite repeated glaciation, certain high-latitude landscapes have remained virtually unchanged for hundreds of thousands or even millions of years. Conversely, low-elevation surfaces have younger minimum limiting ages, although bedrock samples still preserve inheritance and evidence of burial. Boulders at low elevations indicate that deglaciation along the 100-km-long sample transect took place rapidly at a rate of ~120 m yr^{-1} at ca. 11.3 ka, supporting the idea that large bodies of

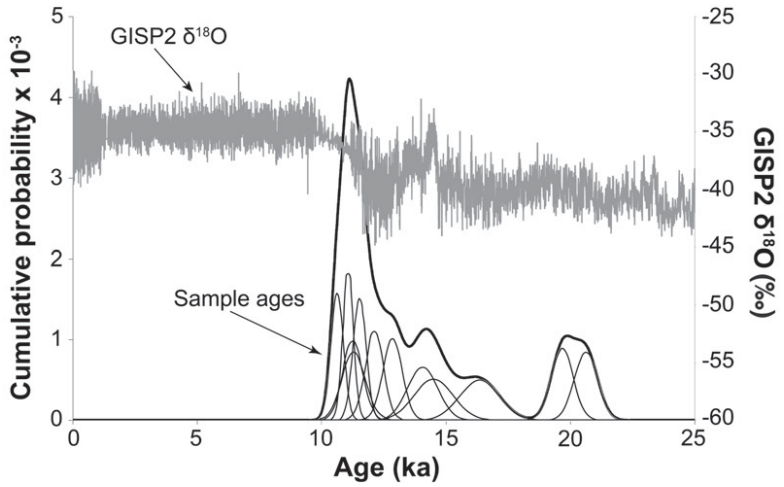

Figure 14. Deglaciation timing and paleoclimate context. Thin black lines show the probability density functions for each individual boulder sample (the oldest boulder sample, 44.3 ka, has been omitted from this plot for better visibility). The thick black line shows the summed cumulative probability for the entire boulder data set. The dark gray line represents δ^{18}O values from the Greenland Ice Sheet Project 2 (GISP2) ice core from Greenland's summit; these data, available online at http://depts.washington.edu/qil/datasets/, are courtesy of M. Stuiver and P.M. Grootes at University of Washington. Minimum limiting ^{10}Be ages are plotted against the left axis, while GISP2 δ^{18}O values are plotted against the right axis.

ice can disintegrate on time scales that would be noticeable and meaningful to humans.

ACKNOWLEDGMENTS

Support for research was provided by the National Science Foundation under award number ARC-0713956 to Bierman and Neumann, a National Science Foundation Graduate Research Fellowship to Corbett, and the University of Vermont. Field support was provided by CH2MHILL Polarfield Services. We thank R.C. Finkel for assistance in measuring ^{26}Al samples and for guidance throughout the project. This work was performed in part under the auspices of the U.S. Department of Energy by Lawrence Livermore National Laboratory under contract DE-AC52-07NA27344. The manuscript was greatly improved by thoughtful reviews from H. Linge and V. Rinterknecht.

REFERENCES CITED

Alley, R., 2000, The Younger Dryas cold interval as viewed from central Greenland: Quaternary Science Reviews, v. 19, p. 213–226, doi:10.1016/S0277-3791(99)00062-1.

Anderson, N., Clarke, A., Juhler, R., McGowan, S., and Renberg, I., 2000, Coring of laminated lake sediments for pigment and mineral magnetic analyses, Sondre Stromfjord, southern West Greenland: Geology of Greenland Survey Bulletin, v. 186, p. 83–87.

Argento, D., Reedy, R., and Stone, J., 2013, Modeling the Earth's cosmic radiation: Nuclear Instruments & Methods in Physics Research, Section B, Beam Interactions with Materials and Atoms, v. 294, p. 464–469, doi:10.1016/j.nimb.2012.05.022.

Atkins, C., Barrett, P., and Hicock, S., 2002, Cold glaciers erode and deposit: Evidence from Allan Hills, Antarctica: Geology, v. 30, no. 7, p. 659–662, doi:10.1130/0091-7613(2002)030<0659:CGEADE>2.0.CO;2.

Balco, G., 2011, Contributions and unrealized potential contributions of cosmogenic-nuclide exposure dating to glacier chronology, 1990–2010: Quaternary Science Reviews, v. 30, no. 1–2, p. 3–27, doi:10.1016/j.quascirev.2010.11.003.

Balco, G., Stone, J., Lifton, N., and Dunai, T., 2008, A complete and easily accessible means of calculating surface exposure ages or erosion rates from ^{10}Be and ^{26}Al measurements: Quaternary Geochronology, v. 3, no. 3, p. 174–195, doi:10.1016/j.quageo.2007.12.001.

Balco, G., Briner, J., Finkel, R., Rayburn, J., Ridge, J., and Schaefer, J., 2009, Regional beryllium-10 production rate calibration for late-glacial northeastern North America: Quaternary Geochronology, v. 4, no. 2, p. 93–107, doi:10.1016/j.quageo.2008.09.001.

Bartoli, G., Sarnthein, M., Weinelt, M., Erlenkeuser, H., Garbe-Schonberg, D., and Lea, D.W., 2005, Final closure of Panama and the onset of Northern Hemisphere glaciation: Earth and Planetary Science Letters, v. 237, p. 33–44, doi:10.1016/j.epsl.2005.06.020.

Bennike, O., 2000, Palaeoecological studies of Holocene lake sediments from west Greenland: Palaeogeography, Palaeoclimatology, Palaeoecology, v. 155, no. 3, p. 285–304, doi:10.1016/S0031-0182(99)00121-2.

Bennike, O., 2008, An early Holocene Greenland whale from Melville Bugt, Greenland: Quaternary Research, v. 69, no. 1, p. 72–76, doi:10.1016/j.yqres.2007.10.004.

Bennike, O., and Björck, S., 2002, Chronology of the last recession of the Greenland Ice Sheet: Journal of Quaternary Science, v. 17, no. 3, p. 211–219, doi:10.1002/jqs.670.

Bierman, P., Marsella, K., Patterson, C., Davis, P., and Caffee, M., 1999, Mid-Pleistocene cosmogenic minimum-age limits for pre-Wisconsinan glacial surfaces in southwestern Minnesota and southern Baffin Island: A multiple nuclide approach: Geomorphology, v. 27, no. 1, p. 25–39, doi:10.1016/S0169-555X(98)00088-9.

Blake, W., 1970, Studies of glacial history in Arctic Canada: Pumice, radiocarbon dates, and differential postglacial uplift in the eastern Queen Elizabeth Islands: Canadian Journal of Earth Sciences, v. 7, p. 634–664, doi:10.1139/e70-065.

Bonow, J., Lidmar-Bergstrom, K., Japsen, P., Chalmers, J., and Green, P., 2007, Elevated erosion surfaces in central West Greenland and southern Norway: Their significance in integrated studies of passive margin development: Norwegian Journal of Geology, v. 87, p. 197–206.

Briner, J., and Swanson, T., 1998, Using inherited cosmogenic ^{36}Cl to constrain glacial erosion rates of the Cordilleran ice sheet: Geology, v. 26, no. 1, p. 3–6, doi:10.1130/0091-7613(1998)026<0003:UICCTC>2.3.CO;2.

Briner, J., Miller, G., Davis, P., Bierman, P., and Caffee, M., 2003, Last Glacial Maximum ice sheet dynamics in Arctic Canada inferred from young erratics perched on ancient tors: Quaternary Science Reviews, v. 22, no. 5–7, p. 437–444, doi:10.1016/S0277-3791(03)00003-9.

Briner, J., Miller, G., Davis, P., and Finkel, R., 2006, Cosmogenic radionuclides from fjord landscapes support differential erosion by overriding ice sheets: Geological Society of America Bulletin, v. 118, no. 3–4, p. 406–420, doi:10.1130/B25716.1.

Briner, J., Bini, A., and Anderson, R., 2009, Rapid early Holocene retreat of a Laurentide outlet glacier through an Arctic fjord: Nature Geoscience, v. 2, p. 496–499, doi:10.1038/ngeo556.

Briner, J., Young, N., Goehring, B., and Schaefer, J., 2012, Constraining Holocene ^{10}Be production rates in Greenland: Journal of Quaternary Science, v. 27, no. 1, p. 2–6, doi:10.1002/jqs.1562.

Corbett, L., Young, N., Bierman, P., Briner, J., Neumann, T., Graly, J., and Rood, D., 2011, Paired bedrock and boulder ^{10}Be concentrations resulting from early Holocene ice retreat near Jakobshavn Isfjord, western Greenland: Quaternary Science Reviews, v. 30, p. 1739–1749, doi:10.1016/j.quascirev.2011.04.001.

Cuffey, K., Conway, H., Gades, A., Hallet, B., Lorrain, R., Severinghaus, J., Steig, E., Vaughn, B., and White, J., 2000, Entrainment at cold glacier beds: Geology, v. 28, no. 4, p. 351–354, doi:10.1130/0091-7613(2000)28<351:EACGB>2.0.CO;2.

Dahl-Jensen, D., Mosegaard, K., Gundestrup, N., Clow, G., Johnsen, S., Hansen, A., and Balling, N., 1998, Past temperatures directly from the Greenland Ice Sheet: Science, v. 282, no. 5387, p. 268–271, doi:10.1126/science.282.5387.268.

Dyke, A., 1979, Quaternary geomorphology, glacial chronology, and climatic and sea-level history of southwestern Cumberland Peninsula, Baffin Island, Northwest Territories, Canada: Arctic and Alpine Research, v. 11, no. 2, p. 179–202, doi:10.2307/1550644.

England, J., 1976, Postglacial isobases and uplift curves from the Canadian and Greenland High Arctic: Arctic and Alpine Research, v. 8, no. 1, p. 61–78, doi:10.2307/1550610.

England, J., 1987, Glaciation and the evolution of the Canadian High Arctic landscape: Geology, v. 15, no. 5, p. 419–423, doi:10.1130/0091-7613(1987)15<419:GATEOT>2.0.CO;2.

Escher, J., and Pulvertaft, T., 1995, Geological Map of Greenland 1:2,500,000: Copenhagen, Denmark, Geologic Survey of Greenland, scale 1:2,500,000.

Fabel, D., and Harbor, J., 1999, The use of in-situ produced cosmogenic radionuclides in glaciology and glacial geomorphology: Annals of Glaciology, v. 28, no. 1, p. 103–110, doi:10.3189/172756499781821968.

Fredskild, B., 1985, The Holocene Vegetational Development of Tugtuligssuaq and Qeqertat, Northwest Greenland: Copenhagen, Museum Tusculanum Press, Monographs on Greenland, 20 p.

Funder, S., and Hansen, L., 1996, The Greenland Ice Sheet—A model for its culmination and decay during and after the Last Glacial Maximum: Bulletin of the Geological Society of Denmark, v. 42, p. 137–152.

Glasser, N., and Ghiglione, M., 2009, Structural, tectonic and glaciological controls on the evolution of fjord landscapes: Geomorphology, v. 105, no. 3–4, p. 291–302, doi:10.1016/j.geomorph.2008.10.007.

Goehring, B., Brook, E., Linge, H., Raisbeck, G., and Yiou, F., 2008, Beryllium-10 exposure ages of erratic boulders in southern Norway and implications for the history of the Fennoscandian Ice Sheet: Quaternary Science Reviews, v. 27, p. 320–336, doi:10.1016/j.quascirev.2007.11.004.

Goehring, B., Kelly, M., Schaefer, J., Finkel, R., and Lowell, T., 2010, Dating of raised marine and lacustrine deposits in east Greenland using beryllium-10 depth profiles and implications for estimates of subglacial erosion: Journal of Quaternary Science, v. 25, no. 6, p. 865–874, doi:10.1002/jqs.1380.

Gosse, J., and Phillips, F., 2001, Terrestrial in situ cosmogenic nuclides: Theory and application: Quaternary Science Reviews, v. 20, no. 14, p. 1475–1560, doi:10.1016/S0277-3791(00)00171-2.

Gosse, J., Grant, D., Klein, J., Klassen, R., Evenson, E., Lawn, B., and Middleton, R., 1993, Significance of altitudinal weathering zones in Atlantic Canada, inferred from in situ produced cosmogenic radionuclides: Geological Society of America Abstracts with Programs, v. 25, no. 6, p. A394.

Gosse, J., Evenson, E., Klein, J., Lawn, B., and Middleton, R., 1995a, Precise cosmogenic ^{10}Be measurements in western North America: Support for a global Younger Dryas cooling event: Geology, v. 23, no. 10, p. 877–880, doi:10.1130/0091-7613(1995)023<0877:PCBMIW>2.3.CO;2.

Gosse, J., Grant, D., Klein, J., and Lawn, B., 1995b, Cosmogenic ^{10}Be and ^{26}Al constraints on weathering zone genesis, ice cap basal conditions, and Long Range Mountain (Newfoundland) glacial history: Proceedings of the Canadian Quaternary Association–Canadian Geomorphology Research Group (CANQUA-CGRC) Conference Abstracts: Memorial University, Saint Johns, Newfoundland, v. CA19.

Granger, D., and Muzikar, P., 2001, Dating sediment burial with in situ–produced cosmogenic nuclides: Theory, techniques, and limitations: Earth and Planetary Science Letters, v. 188, no. 1–2, p. 269–281, doi:10.1016/S0012-821X(01)00309-0.

Håkansson, L., Briner, J., Alexanderson, H., Aldahan, A., and Possnert, G., 2007, ^{10}Be ages from central east Greenland constrain the extent of the Greenland Ice Sheet during the Last Glacial Maximum: Quaternary Science Reviews, v. 26, no. 19–21, p. 2316–2321, doi:10.1016/j.quascirev.2007.08.001.

Håkansson, L., Alexanderson, H., Hjort, C., Moller, P., Briner, J., Aldahan, A., and Possnert, G., 2008, Late Pleistocene glacial history of Jameson Land, central east Greenland, derived from cosmogenic ^{10}Be and ^{26}Al exposure dating: Boreas, v. 38, no. 2, p. 244–260, doi:10.1111/j.1502-3885.2008.00064.x.

Harbor, J., 1992, Numerical modeling of the development of U-shaped valleys by glacial erosion: Geological Society of America Bulletin, v. 104, p. 1364–1375, doi:10.1130/0016-7606(1992)104<1364:NMOTDO>2.3.CO;2.

Harbor, J., Stroeven, A., Fabel, D., Clarhäll, A., Kleman, J., Li, Y., Elmore, D., and Fink, D., 2006, Cosmogenic nuclide evidence for minimal erosion across two subglacial sliding boundaries of the late glacial Fennoscandian ice sheet: Geomorphology, v. 75, no. 1–2, p. 90–99, doi:10.1016/j.geomorph.2004.09.036.

Herman, F., Beaud, F., Champagnac, J., Lemieux, J., and Sternai, P., 2011, Glacial hydrology and erosion patterns: A mechanism for carving glacial valleys: Earth and Planetary Science Letters, v. 310, p. 498–508, doi:10.1016/j.epsl.2011.08.022.

Hughes, A., Rainsley, E., Murray, T., Fogwill, C., Schnabel, C., and Xu, S., 2012, Rapid response of Helheim Glacier, southeast Greenland, to early Holocene climate warming: Geology, v. 40, no. 5, p. 427–430, doi:10.1130/G32730.1.

Kelly, M., 1980, Preliminary investigations of the Quaternary of Melville Bugt and Dundas, northwest Greenland: Rapport Gronlands Geologiske Undersogelse, v. 100, p. 33–38.

Kelly, M., Lowell, T., Hall, B., Schaefer, J., Finkel, R., Goehring, B., Alley, R., and Denton, G., 2008, A ^{10}Be chronology of late glacial and Holocene mountain glaciation in the Scoresby Sund region, east Greenland: Implications for seasonality during late glacial time: Quaternary Science Reviews, v. 27, p. 2273–2282, doi:10.1016/j.quascirev.2008.08.004.

Kleman, J., 1992, The palimpsest glacial landscape in northwestern Sweden: Late Weichselian deglaciation landforms and traces of older west-centered ice sheets: Geografiska Annaler, ser. A, Physical Geography, v. 74, no. 4, p. 305–325, doi:10.2307/521429.

Kleman, J., and Borgstrom, I., 1994, Glacial land forms indicative of a partly frozen bed: Journal of Glaciology, v. 40, no. 135, p. 255–264.

Lal, D., 1988, In situ–produced cosmogenic isotopes in terrestrial rocks: Annual Review of Earth and Planetary Sciences, v. 16, no. 1, p. 355–388, doi:10.1146/annurev.ea.16.050188.002035.

Lal, D., 1991, Cosmic ray labeling of erosion surfaces: In situ nuclide production rates and erosion models: Earth and Planetary Science Letters, v. 104, no. 2–4, p. 424–439, doi:10.1016/0012-821X(91)90220-C.

Lilly, K., Fink, D., Fabel, D., and Lambeck, K., 2010, Pleistocene dynamics of the interior of the East Antarctic ice sheet: Geology, v. 38, no. 8, p. 703–706, doi:10.1130/G31172x.1.

Lisiecki, L., and Raymo, M., 2005, A Plio-Pleistocene stack of 57 globally distributed benthic ^{18}O records: Paleoceanography, v. 20, p. 522–533.

Long, A., and Roberts, D., 2003, Late Weichselian deglacial history of Disko Bugt, West Greenland, and the dynamics of the Jakobshavns Isbrae ice stream: Boreas, v. 32, no. 1, p. 208–226.

Long, A., Roberts, D., and Dawson, S., 2006, Early Holocene history of the West Greenland ice sheet and the GH-8.2 event: Quaternary Science Reviews, v. 25, p. 904–922, doi:10.1016/j.quascirev.2005.07.002.

Mangerud, J., Goehring, B., Lohne, O., Svendsen, J., and Gyllencreutz, R., 2013, Collapse of marine-based outlet glaciers from the Scandinavian Ice Sheet: Quaternary Science Reviews, v. 67, p. 8–16, doi:10.1016/j.quascirev.2013.01.024.

Marquette, G., Gray, J., Gosse, J., Courchesne, F., Stockli, L., MacPherson, G., and Finkel, R., 2004, Felsenmeer persistence under non-erosive ice in the Torngat and Kaumajet Mountains, Quebec and Labrador, as determined by soil weathering and cosmogenic nuclide exposure dating: Canadian Journal of Earth Sciences, v. 41, no. 1, p. 19–38, doi:10.1139/e03-072.

Nishiizumi, K., 2004, Preparation of ^{26}Al AMS standards: Nuclear Instruments & Methods in Physics Research, Section B, Beam Interactions with Materials and Atoms, v. 223–224, p. 388–392, doi:10.1016/j.nimb.2004.04.075.

Nishiizumi, K., Winterer, E., Kohl, C., Klein, J., Middleton, R., Lal, D., and Arnold, J., 1989, Cosmic ray production rates of ^{10}Be and ^{26}Al in quartz from glacially polished rocks: Journal of Geophysical Research, v. 94, no. B12, v. 94, no B12, p. 17,907–17,915, doi:10.1029/JB094iB12p17907.

Nishiizumi, K., Kohl, C., Arnold, J., Klein, J., Fink, D., and Middleton, R., 1991, Cosmic ray produced ^{10}Be and ^{26}Al in Antarctic rocks: Exposure and erosion history: Earth and Planetary Science Letters, v. 104, no. 2–4, p. 440–454, doi:10.1016/0012-821X(91)90221-3.

Nishiizumi, K., Imamura, M., Caffee, M., Southon, J., Finkel, R., and McAninch, J., 2007, Absolute calibration of ^{10}Be AMS standards: Nuclear Instruments & Methods in Physics Research, Section B, Beam Interactions with Materials and Atoms, v. 258, no. 2, p. 403–413, doi:10.1016/j.nimb.2007.01.297.

Perren, B., Anderson, N., Douglas, M., and Fritz, S., 2012, The influence of temperature, moisture, and eolian activity on Holocene lake development in West Greenland: Journal of Paleolimnology, v. 48, p. 223–239, doi:10.1007/s10933-012-9613-6.

Peterson, R., 2003, Settlements, Kinship and Hunting Grounds in Traditional Greenland: Copenhagen, Museum Tusculanum Press, 327 p.

Phillips, F., Zreda, M., Smith, S., Elmore, D., Kubik, P., and Sharma, P., 1990, Cosmogenic chlorine-36 chronology for glacial deposits at Bloody Canyon, eastern Sierra Nevada: Science, v. 248, no. 4962, p. 1529–1532, doi:10.1126/science.248.4962.1529.

Phillips, W., Hall, A., Mottram, R., Fifield, L., and Sugden, D., 2006, Cosmogenic ^{10}Be and ^{26}Al exposure ages of tors and erratics, Cairngorm Mountains, Scotland: Timescales for the development of a classic landscape of selective linear glacial erosion: Geomorphology, v. 73, p. 222–245, doi:10.1016/j.geomorph.2005.06.009.

Rinterknecht, V., Gorokhovich, Y., Schaefer, J., and Caffee, M., 2009, Preliminary ^{10}Be chronology for the last deglaciation of the western margin of the Greenland Ice Sheet: Journal of Quaternary Science, v. 24, no. 3, p. 270–278, doi:10.1002/jqs.1226.

Roberts, D., Long, A., Schnabel, C., Freeman, S., and Simpson, M., 2008, The deglacial history of southeast sector of the Greenland Ice Sheet during the Last Glacial Maximum: Quaternary Science Reviews, v. 27, p. 1505–1516, doi:10.1016/j.quascirev.2008.04.008.

Roberts, D., Long, A., Schnabel, C., Davies, B., Xu, S., Simpson, M., and Huybrechts, P., 2009, Ice sheet extent and early deglacial history of the southwestern sector of the Greenland Ice Sheet: Quaternary Science Reviews, v. 28, p. 2760–2773, doi:10.1016/j.quascirev.2009.07.002.

Rood, D., Hall, S., Guilderson, T., Finkel, R., and Brown, T., 2010, Challenges and opportunities in high-precision Be-10 measurements at CAMS: Nuclear Instruments & Methods in Physics Research, Section B, Beam Interactions with Materials and Atoms, v. 268, no. 7–8, p. 730–732, doi:10.1016/j.nimb.2009.10.016.

Schildgen, T., Phillips, W., and Purves, R., 2005, Simulation of snow shielding corrections for cosmogenic nuclide surface exposure studies: Geomorphology, v. 64, no. 1–2, p. 67–85, doi:10.1016/j.geomorph.2004.05.003.

Stone, J., 2000, Air pressure and cosmogenic isotope production: Journal of Geophysical Research, v. 105, no. B10, p. 23,753–23,759, doi:10.1029/2000JB900181.

Stone, J., and Ballantyne, C., 2006, Dimensions and deglacial chronology of the Outer Hebrides Ice Cap, northwest Scotland: Implications of cosmic ray exposure dating: Journal of Quaternary Science, v. 21, no. 1, p. 75–84, doi:10.1002/jqs.933.

Stone, J., Balco, G., Sugden, D., Caffee, M., Sass, L., III, Cowdery, S., and Siddoway, C., 2003, Holocene deglaciation of Marie Byrd Land, West Antarctica: Science, v. 299, no. 5603, p. 99–102, doi:10.1126/science.1077998.

Straneo, F., Sergienko, O., and Heimbach, P., 2012, Understanding the Dynamic Response of Greenland's Marine Terminating Glaciers to Oceanic and Atmospheric Forcing: U.S. Climate Variability and Predictability Working Group Report 2012–2, 23 p.

Stroeven, A., Fabel, D., Harbor, J., Hattestrand, C., and Kleman, J., 2002a, Quantifying the erosional impact of the Fennoscandian ice sheet in the Torneträsk-Narvik corridor, northern Sweden, based on cosmogenic radionuclide data: Geografiska Annaler, ser. A, Physical Geography, v. 84, no. 3–4, p. 275–287, doi:10.1111/j.0435-3676.2002.00182.x.

Stroeven, A., Fabel, D., Hattestrand, C., and Harbor, J., 2002b, A relict landscape in the centre of Fennoscandian glaciation: Cosmogenic radionuclide evidence of tors preserved through multiple glacial cycles: Geomorphology, v. 44, no. 1–2, p. 145–154, doi:10.1016/S0169-555X(01)00150-7.

Stuiver, M., and Grootes, P., 2000, GISP2 oxygen isotope ratios: Quaternary Research, v. 53, no. 3, p. 277–284, doi:10.1006/qres.2000.2127.

Sugden, D., 1977, Reconstruction of the morphology, dynamics, and thermal characteristics of the Laurentide ice sheet at its maximum: Arctic and Alpine Research, v. 9, no. 1, p. 21–47, doi:10.2307/1550407.

Sugden, D., 1978, Glacial erosion by the Laurentide ice sheet: Journal of Glaciology, v. 20, no. 83, p. 367–391.

Sugden, D., and Watts, S., 1977, Tors, felsenmeer, and glaciation in northern Cumberland Peninsula, Baffin Island: Canadian Journal of Earth Sciences, v. 14, no. 12, p. 2817–2823, doi:10.1139/e77-248.

Sugden, D., Balco, G., Cowdery, S., Stone, J., and Sass, L., III, 2005, Selective glacial erosion and weathering zones in the coastal mountains of Marie Byrd Land, Antarctica: Geomorphology, v. 67, no. 3–4, p. 317–334, doi:10.1016/j.geomorph.2004.10.007.

Swift, D., Persano, C., Stuart, F., Gallagher, K., and Whitham, A., 2008, A reassessment of the role of ice sheet glaciation in the long-term evolution of the east Greenland fjord region: Geomorphology, v. 97, no. 1–2, p. 109–125, doi:10.1016/j.geomorph.2007.02.048.

Taylor, K., Lamorey, G., Doyle, G., Alley, R., Grootes, P., Mayewski, P., White, J., and Barlow, L., 1993, The 'flickering switch' of late Pleistocene climate change: Nature, v. 361, p. 432–436, doi:10.1038/361432a0.

Taylor, K., Mayewski, P., Alley, R., Brook, E., Gow, A., Grootes, P., Meese, D., Saltzman, E., Severinghaus, J., and Twickler, M., 1997, The Holocene–Younger Dryas transition recorded at Summit, Greenland: Science, v. 278, no. 5339, p. 825–827, doi:10.1126/science.278.5339.825.

Ten Brink, N., 1974, Glacio-isostasy: New data from West Greenland and geophysical implications: Geological Society of America Bulletin, v. 85, p. 219–228, doi:10.1130/0016-7606(1974)85<219:GNDFWG>2.0.CO;2.

Waller, R., Murton, J., and Kristensen, L., 2012, Glacier–permafrost interactions: Processes, products and glaciological implications: Sedimentary Geology, v. 255–256, p. 1–28, doi:10.1016/j.sedgeo.2012.02.005.

Young, N., Briner, J., Stewart, H., Axford, Y., Csatho, B., Rood, D., and Finkel, R., 2011, Response of Jakobshavn Isbrae, Greenland, to Holocene climate change: Geology, v. 39, no. 2, p. 131–134, doi:10.1130/G31399.1.

Science Editor: Christian Koeberl

Associate Editor: Benjamin J.C. Laabs

Manuscript Received 31 October 2012
Revised Manuscript Received 28 March 2013
Manuscript Accepted 22 April 2013

Printed in the USA